Elsevier Editorial System(tm) for Mechanism and Machine Theory

Manuscript Draft

Manuscript Number: MECHMT-D-16-00336R2

Title: Analysis and synthesis of LinWWC-VSA, a variable stiffness actuator for linear motion

Article Type: Research paper

Keywords: Variable Stiffness Actuator; Linear motion; Spiral cam; Logarithmic spiral

Corresponding Author: Dr. Matteo Malosio, Ph.D.

Corresponding Author's Institution: Italian National Research Council

First Author: Giulio Spagnuolo, M.S.

Order of Authors: Giulio Spagnuolo, M.S.; Matteo Malosio, Ph.D.; Tito Dinon, M.S.; Lorenzo Molinari Tosatti, Ph.D.; Giovanni Legnani, Ph.D.

Abstract: This work presents the principle of operation of LinWWC-VSA, a Variable Stiffness Actuator (VSA) suitable to perform linear motions, conversely to the vast majority of VSAs typically designed to perform rotational movements and often affected by limits in the actually exploitable range of motions. It features two antagonist nonlinear equivalent springs, each of them made up of a cam wrapped by a wire and constrained by a torsion spring. This work presents methods both for the analysis and the synthesis of the actuator. Two synthesis methods, one numerical and one analytic, are described to design the cam profile as function of the desired stiffness-displacement characteristic of each equivalent nonlinear spring. The analytic method exploits the peculiar formulation of the logarithmic spiral. The theoretical aspects of the actuator are accompanied by numerical simulations.

# Authors' Response to the Review Comments

***Journal:*** Mechanism and Machine Theory

***Manuscript #:*** MECHMT-D-16-00336

***Title of Paper:*** Analysis and synthesis of LinWWC-VSA, a variable stiffness actuator for linear motion

***Authors:*** Giulio Spagnuolo, Matteo Malosio, Tito Dinon, Lorenzo Molinari Tosatti, Giovanni Legnani

***Date Sent:*** October 27th, 2016

We greatly appreciate the time and efforts by the editor and referees in reviewing this manuscript. We have addressed the issues indicated in the review report, in the hope that the revised version can meet the journal publication requirements.

## Response to Comments from Reviewer 1

### Overall Comment

*This paper deals with the design details (concept, synthesis, and analysis) of a simple but very interesting embodiment for achieving a variable stiffness in a linear actuator.*

*The paper is well organized and well written. It is complete and methodologically clear. The paper deals with both theoretical issues and practical implementation and, therefore, it can be a valuable contribution.*

*My opinion is that the authors can now focus on making the paper suitable for publication in an archival journal.*

*Some changes must be made by the author to improve the final quality of the manuscript.*

### Response

The authors would like to thank Reviewer 1.

### Comment 1

*As a general comment, the style of the equation parameters must be made uniform and compliant to the standards of the journal.*

*As an example, vectors are in some cases denoted by a bold upright letter (e.g. page 5), in other cases they are denoted by an italic capital letter with arrows (e.g. page 10), and in other cases with a simple sign (e.g. page 11).*

## Response

Bold upright letters, denoting vectors, have been substituted by italic lowercase letters with arrows, for coherency with other symbols. Italic capital letters denote points, this has been underlined adding a row in the Table1. As reported in Table 1, two italic capital letters with arrows denote an infinite line containing point A and point B, not vectors. Similarly, two italic capital letters with a simple sign denote a segment from point A to point B. The word "line" in Table 1 has been substituted by "line segment" in this revised version.

## Comment 2

*The inextensibility of the wire has to be clearly pointed out by the author in the assumption of the model.*

## Response

The wire inextensibility has been pointed out in some sentences of Section 3. In particular:

- in the caption of Figure 5;
- in the sentence "Referring to Fig. 5 let us consider the cam *c* wrapped by an inextensible wire *w*,…";
- in the sentence "Referring to Fig. 7 and considering the wire inextensibility,...".

## Comment 3

*It is not clear why the solution with rollers to adjust the location of the output end of the wire is neglected in the prototypes and renderings at the end of the paper.*

## Response

It was neglected in the first version for simplicity of the drawing. In the revised version of the paper, rollers have been included in Figure 19. The carriage of the prototype depicted in Figure 20 is now transparent and the rollers are notable. They were present also in the first version of the paper but since the carriage was opaque they were hidden. Rollers were already present in Figure 22; in this revised version they have been highlighted in white.

## Comment 4

*Is it possible to obtain an alternative practical solution without aligning rollers?*

## Response

Figure 19 shows now two alternative solutions.

Figure 19(a) is characterized by coplanar wires. Fig. 19(b) is an alternative solution with coaxial cams. This configuration allows to obtain a more compact solution, with the drawback, negligible in many cases, that

the two antagonist forces are not coplanar. Thanks to its compactness, this second configuration is the one embedded inside the prototype LINarm2 illustrated in Fig.20.

This explanation has been included in the section Conclusions and in the caption of Figure 19.

## Specific comment 1

*Avoid the reference to the founding source in the title. This should be postponed until the acknowledgement.*

## Response

The reference to the founding source has been moved to the acknowledgment section.

## Specific comment 2

*Please check if specific publication policies (i.e. open access) of the European Commission must be followed.*

## Response

The authors are free to choose the publication policy. They will probably ask for the open-access policy.

## Specific comment 3

*The dotted curve in Figure 11 can be confused with the circumferential and radial grid.*

## Response

The dotted line has been converted in a line with "x" markers. We hope it is acceptable.

## Specific comment 4

*The dotted curves in Figure 12 are too light and their visibility should be improved.*

## Response

The dotted curves have been converted in curves with "x" markers. We hope it is acceptable.

## Specific comment 5

*Units (within the text and in all the Figures) must be written in upright characters (not italic).*

## Response

Units have been substituted with upright characters (not italic).

## Specific comment 6

*Some units are missing in Table 3 (e.g. radians in the third entry).*

## Response

The units of the third and of the fifth entries have been added and, specifically, are rad and $rad^{-1}$. The

"unitless" quantity in the first entry (it is a ratio between two stiffness) have been denoted by --. The authors judged that (N/m)/(N/m) is a bit verbose.

### Specific comment 7

*Page 15 change "independently of" into "independently from".*

### Response

Thank you. We've corrected it.

### Specific comment 8

*The curves in the plots of Fig. 16 are too light. Especially in subplot a, this line-weight causes the curve to disappear into the grid.*

### Response

In order not to change the uniformity with line styles in previous graphs (one continuous and one dashed line in each graph), instead of modifying the styles of the lines we have modified the grid changing its color from black to gray, in order to increase the visibility of the dotted line in Fig.16a. We hope it is acceptable.

### Specific comment 9

*The acknowledgement section must taken be out of the reference section.*

### Response

We have moved it before the Reference section.

## Response to Comments from Reviewer 2

### Overall Comment

*The paper present the architecture, design, and analysis procedures for a variable stiffness actuator for linear motion.*

*The paper is well written and clear and, in the opinion of this reviewer, the paper is suitable for publication in the Journal of Mechanism and Machine theory.*

### Response

The authors would like to thank Reviewer 2.

**Graphical Abstract (for review)**

# Highlights

- The concept design of a variable stiffness actuator for linear motion is proposed.
- The mechanism exploits a wire-based mechanical transmission and spiral-shaped cams.
- The equations to analyze the mechanism are presented.
- Two synthesis methods, one analytic and one numerical, are explained are simulation results are reported.
- Examples of use in real prototypes are illustrated.

# Analysis and synthesis of LinWWC-VSA, a variable stiffness actuator for linear motion

G. Spagnuolo[a,b,1], M. Malosio[a,1,*], T. Dinon[a], L. Molinari Tosatti[a], G. Legnani[a,b]

[a] *Institute of Industrial Technologies and Automation - CNR, via Alfonso Corti 12, 20133 Milan, Italy*
[b] *University of Brescia, Piazza del Mercato 15, 25121 Brescia, Italy*

**Abstract**

This work presents the principle of operation of LinWWC-VSA, a Variable Stiffness Actuator (VSA) suitable to perform linear motions, conversely to the vast majority of VSAs typically designed to perform rotational movements and often affected by limits in the actually exploitable range of motions. It features two antagonist nonlinear equivalent springs, each of them made up of a cam wrapped by a wire and constrained by a torsion spring. This work presents methods both for the analysis and the synthesis of the actuator. Two synthesis methods, one numerical and one analytic, are described to design the cam profile as function of the desired stiffness-displacement characteristic of each equivalent nonlinear spring. The analytic method exploits the peculiar formulation of the logarithmic spiral. The theoretical aspects of the actuator are accompanied by numerical simulations.

*Keywords:*
Variable Stiffness Actuator, Linear motion, Spiral cam, Logarithmic spiral

## 1. Introduction

### *1.1. Variable Stiffness Actuators*

A Variable Impedance Actuator (VIA) is an actuator which deviates from its set equilibrium position, depending on the external forces and the mechanical properties of the actuator (i.e. inertia, stiffness and damping factors), oppositely to non-VIA (traditional stiff actuator) characterized by excellent trajectory tracking with a high bandwidth and high accuracy [1]. Inherent compliance actuators constitute a subgroup of VIAs, containing passive or intrinsic compliant element in series to the (stiff) actuator. They can be subdivided into Series Elastic Actuators (SEA - Fig. 1a) [2], in which the compliant element does not change its stiffness (fixed compliance), and Variable Stiffness Actuators (VSA - Fig. 1b) [3], in which the stiffness is controlled by mechanical reconfiguration.

*Corresponding author
*Email address:* matteo.malosio@itia.cnr.it (M. Malosio)
[1] These authors contributed equally to this work.

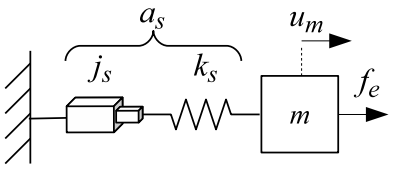


(a) Series Elastic Actuator (SEA).

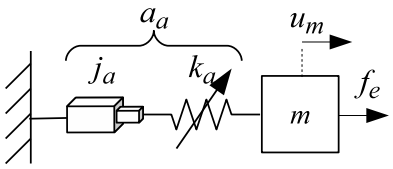


(b) Variable Stiffness Actuator (VSA).

Figure 1: A Series Elastic Actuator $a_s$ is made up of an actuator $j_s$ and a compliant element $k_s$ configured in series. A Variable Stiffness Actuator $a_a$ is characterized by an adjustable compliant element $k_a$. An external force $f_e$ applied to $m$ causes a displacement $u_m$.

VSAs [1] allow the adjustment, in a controlled manner and at the same time, of both the mechanical stiffness and the equilibrium configuration of the load. Peculiar features are mechanical stiffness adjustment, adaptability and force accuracy in the interaction with the operator facilitating a direct interaction with humans limiting forces in case of collision, and robustness to external perturbations or model errors [4]. All of them are obtained without necessarily requiring force-based control techniques, favoring mechanical backdrivability and transparency.

For all these aspects, potentially positive in a number of applications, a number of different VSAs have been conceived and realized in the last years [1, 5, 6]. Moreover, the more and more growing interest in VSAs led Grioli et al. to present a VSA datasheet as an interface language between designers and users and to discuss design procedures and how VSA data may be organized to minimize the engineers effort in choosing the actuator type and size [7]. In order to further support designers in developing new VSA solutions, design guidelines for R&D engineers facing the challenge of designing new VSA systems and implementing them in use-cases as shock absorbing, stiffness variation, cyclic motions and explosive motions are proposed [6].

### *1.2. Use of VSA to realize linear motions*

It is a matter of fact that the vast majority of the so-far developed VSAs perform rotational motions. In order to realize linear motions using rotational actuators, it is common the use of transmissions based on rack and pinion, pulley and belt, or drum and wire. These solutions are all valid but, with the purpose of realizing linear actuators with (theoretically) no stroke restrictions, the employed actuators require not to be affected by any rotational limit or end stroke (i.e. they should be able to perform an unlimited number of turns). While this is a characteristic taken for granted for common rotational motors, it is not for VSA rotational actuators. In fact, only few rotational VSAs have so far being developed featuring an infinite number of turns. Among them it is worth to mention the PVSA [8], the actuator developed by Tonietti et al. [9] and the ComPact-VSA [10]. However, all of them requires a great number of manufactured parts. The first two are moreover characterized by the presence of a pin-slot joint which requires precise manufacturing and assembling operations. It is worth moreover to mention the vsaUT-II [11] which guarantees a large variation of stiffness but requires many manufactured components and mechanical joints as

gears and pin-slot joints. It is moreover affected by a limited rotational range of motion.

The use of profiled surfaces can be promising in order to customize the stiffness-displacement curve. Both the VS-Joint mechanism [12] and the third VSA presented by Guo et al. in [13] require a pin-slot joint and good mechanical tolerances. Interesting is AMASC [14] which exploits coupled cams to obtain springs non-linearity.

In conclusion, few rotational VSAs can be effectively exploited to realize linear motions without (theoretically) any stroke limit and they are typically characterized by a great number of components and require strict-tolerance machining and assembling operations to avoid backlashes or jammings.

### *1.3. The Linear Wire-Wrapped Cam VSA*

This work aims at presenting and analyzing the operating mechanism of the Linear Wire-Wrapped Cam VSA (LinWWC-VSA), an Agonist-Antagonist VSA (AAVSA) [3, 4] suitable to realize linear axes with a theoretically infinite stroke. It is made up of two antagonistic LinWWC-SEA, each of them featuring a cam wrapped by a wire and constrained by a torsion spring, realizing an equivalent tension spring characterized by a customizable non-linear stiffness characteristic. The use of a cam wrapped by a wire is considered promising in order to minimize the number of mechanical components, as better described in next sections, simplifying the design and assembly operations, and limiting concentrated mechanical stresses. Examples of employment of this approach are the MACCEPA 2.0 [15], the pnrVSA [16], the one proposed by Shin et al. [17] actuated by pneumatic artificial muscles and the NLSs proposed by Schepelmann et al. [18]. However, all of them are configured to perform rotational movements characterized by a limited rotational range of motion, not directly applicable to realize linear motions without any inherent stroke limitation.

The intrinsic simplicity of LinWWC-VSA allows it to be realized assembling affordable off-the-shelf components together with components manufacturable by low-cost techniques as table-top entry-level 3d-printers. The few number of required components contributes to realize an overall affordable solution.

The work is organized as follows. The list of used symbols is reported in Table 1. General aspects about AAVSA exploited in subsequent sections are introduced in Section 2. The LinWWC-SEA is analyzed in Section 3. The LinWWC-VSA is depicted in Section 4. Both numerical and analytic methodologies to synthesize the shape of the cam are detailed in Section 5. Simulations and related discussions are reported in Section 6. Conclusions and future works are drawn in Section 7.

## 2. General aspects of Agonist-Antagonist VSAs

An Agonist-Antagonist VSA (AAVSA) mimics the principle at the basis of antagonist muscles [19], for which the stronger the antagonistic forces are, the stiffer the articulation becomes [5]. It is made up of two antagonist SEAs, kinematically in parallel with respect to a mobile mass (Fig. 2). The non-linearity of the elastic element is required to allow the adjustment of the VSA stiffness [4].

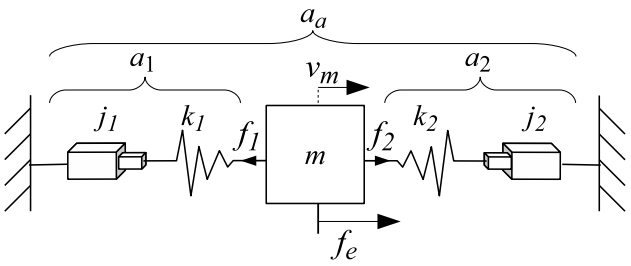


Figure 2: Typical scheme of an antagonistic VSA: two antagonist non-linear SEAs $a_i$ control the position and the stiffness of a mobile mass $m$.

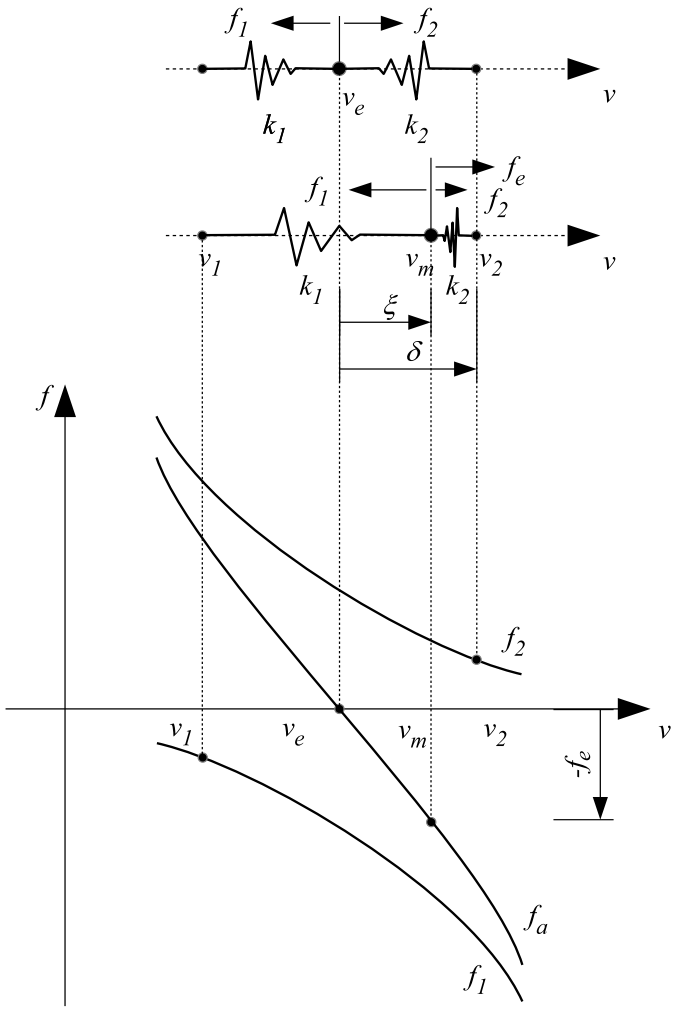


Figure 3: Force characteristic of a VSA as function of the ground end-points $u_1, u_2$ of springs $k_1, k_2$ and of the external force $f_e$.

Referring to Fig. 1 let us denote by $a$ a generic compliant actuator made up of a rigid joint $j$ and a spring $s$ with stiffness $k$, connected to a mass $m$. Let us conveniently denote

Table 1: Table of symbols

| Symbol | Description |
|---|---|
| $\{k\}$ | Frame of reference |
| $O_k$ | Origin of $\{k\}$ |
| $x_k, y_k$ | Axes of $\{k\}$ |
| $\vec{f}$ | Vector |
| $f$ | Magnitude of vector $\vec{f}$ |
| $\overleftrightarrow{AB}$ | Infinite line containing point $A$ and point $B$ |
| $\overline{AB}$ | Line segment from point $A$ to point $B$ |
| $\angle(AOB), \angle(l_1 l_2)$ | Counterclockwise angle between points $A$ and $B$ at point $O$ (the vertex) or between lines $l_1$ and $l_2$ |
| $r_P^k, \theta_P^k$ | Polar coordinates of $P$ wrt $\{k\}$ |
| $d(P, Q)$ | Distance between point $P$ and $Q$ (i.e. $\|\overrightarrow{PQ}\|$) |
| $d(P, l)$ | Minimum distance between point $P$ and line $l$ |
| $a \propto b$ | $a$ proportional to $b$ |

by the subscripts $s$ and $a$ a SEA (Fig. 1a) and a VSA (Fig. 1b), respectively. Let us denote by $u_m$ the coordinate of $m$, by $u_e$ its coordinate if no external force applied (equilibrium position) and by $\Delta u_m = u_m - u_e$ the displacement of $m$ from its equilibrium position. The stiffness of the actuator and the exerted force are expressed by

$$k(u) = \frac{\mathrm{d}f_a}{\mathrm{d}u} \qquad\qquad f_a = \int_{\Delta u} k(u)\,\mathrm{d}u. \tag{1}$$

In static conditions or neglecting inertial effects of $m$, it is $\vec{f_a} = -\vec{f_e}$, where $\vec{f_a}$ denotes the force exerted by the actuator and $\vec{f_e}$ denotes the external force. Therefore, by knowing the stiffness-displacement curve of $k$ and the position of $m$, it is possible to estimate $f_e$.

Let us now consider a generic AAVSA $a_a$ made up of two antagonist SEA $a_i$ with $i = 1, 2$ (Fig. 2). Each $a_i$ is made up of a rigid joint $j_i$ and a compliant element with stiffness $k_i$. The antagonistic actuators are connected to a mass $m$ with position $v_m$.

Referring to Fig. 3, the force applied to $m$ by $a_a$ is

$$\vec{f_a} = \vec{f_2} + \vec{f_1} = -\vec{f_e}, \qquad f_a = f_2 - f_1 = -f_e. \tag{2}$$

Similarly, being the two actuators kinematically in parallel, the stiffness of $a_a$ is

$$k_a = k_2 + k_1. \tag{3}$$

The force/displacement characteristic of a generic AAVSA given $k_1 = k_2$ is represented in Fig. 3. The equilibrium position of $m$ is determined by the value $-f_e$ along the curve $f_a$ (neglecting inertial effects). If no external force is applied (i.e. $f_e = 0$), the position of $m$ is

$$v_e = (v_1 + v_2)/2. \tag{4}$$

Let us conveniently denote

$$\delta = (v_2 - v_1)/2 \qquad \xi = v_m - v_e \tag{5}$$

used in the next sections as the two independent coordinates of a AAVSA. It is worth to underline that, if $\delta$ and $\xi$ are known, together with the spring stiffness $k(u)$, it is straightforward to deduce $f_e$.

## 3. LinWWC-SEA

Referring to Fig. 4 and to symbols reported in Table 1, let us consider a cam defined by the curve $c$ defined by the polar coordinates $(r, \theta)$ wrt the reference frame $\{c\}$. Let us conveniently consider a cam shaped as a spiral, with $r$ monotonically increasing with respect to $\theta$. Let us denote by $A(r_A, \theta_A)$ and $B(r_B, \theta_B)$ the points of the cam with the minimum and maximum values of $r$, respectively. It is $r_A \leq r \leq r_B$ and $\theta_A \leq \theta \leq \theta_B$. Considering a point $T \in c$, let us denote by $t$ the line passing through $T$ and tangent to $c$, and by $H$ the point on $t$ at minimum distance $b$ from $O_c$.

As it is known in geometry, the curvilinear coordinate of $T(r_T, \theta_T)$ along the cam profile is

$$s_T^A = \int_{\theta_A}^{\theta_T} \mathrm{d}s = \int_{\theta_A}^{\theta_T} \sqrt{r^2 + \left(\frac{\mathrm{d}r}{\mathrm{d}\theta}\right)^2}\, \mathrm{d}\theta \tag{6}$$

and the pitch angle $\beta$, complement of the angle between $t$ and $r$, is equal to

$$\beta = \angle(HO_cT) = \arctan\left(\frac{1}{r}\frac{\mathrm{d}r}{\mathrm{d}\theta}\right). \tag{7}$$

The minimum distance between $t$ and $O_c$ is

$$b = \overline{O_cH} = r\cos\beta. \tag{8}$$

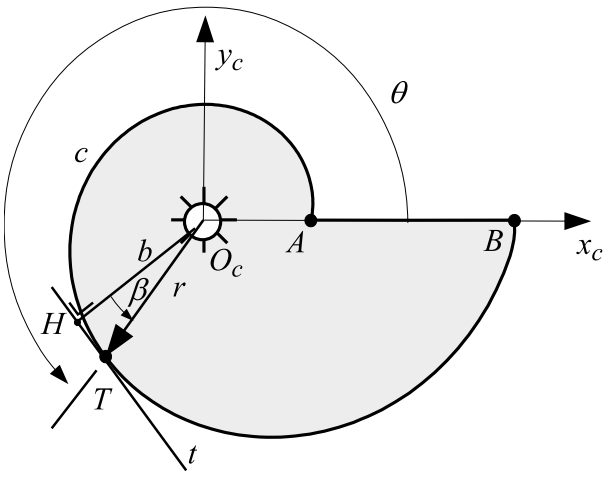


Figure 4: Spiral cam profile.

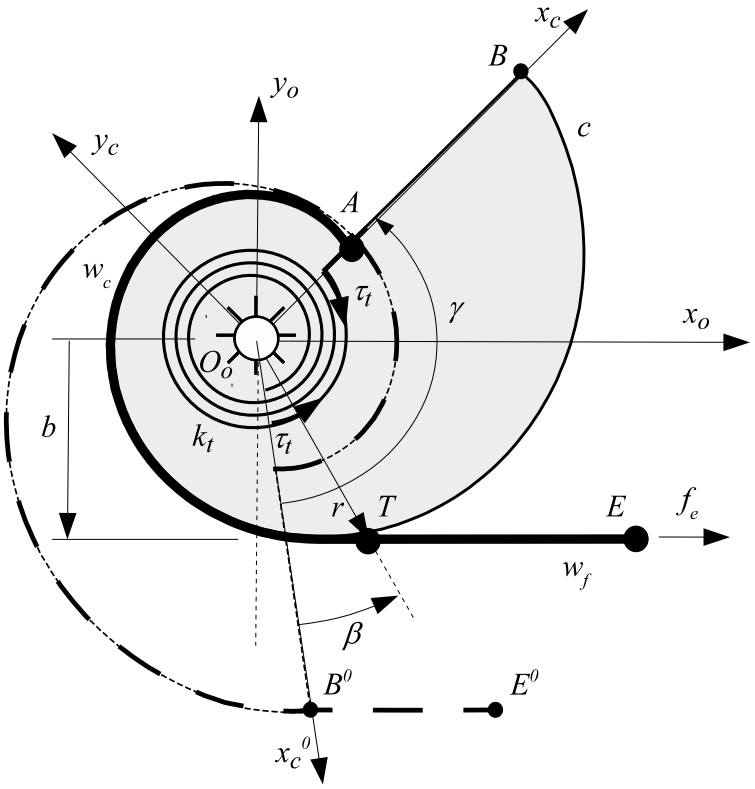


Figure 5: LinWWC-SEA: a non-linear spring obtained by a cam wrapped by an inextensible wire and constrained by a torsion spring. The thicker line represents the wire $w$.

Referring to Fig. 5 let us consider the cam $c$ wrapped by an inextensible wire $w$, with an endpoint constrained to $A$ and the other endpoint $E$ free. Let us denote by $T$ the point in which $w$ is tangent to $c$ and split $w$ in two parts: $w_c$ is wrapped on $c$ between $A$ and $T$, $w_f$ is free between $T$ and $E$. Hence, it is $w = w_c + w_f$, denoting by $w$ both the whole wire and its length for brevity.

Considering a fixed frame $\{o\}$, let us consider the cam hinged in $O_o$ with $O_c \equiv O_o$. The free rotation of the cam is restrained by a torsion spring with stiffness $k_t$ and exerting the torque $\tau_t(\gamma)$:

$$k_t = \frac{\mathrm{d}\tau_t}{\mathrm{d}\gamma} \qquad\qquad \tau_t(\gamma) = \int_\gamma k_t \,\mathrm{d}\gamma + \tau_{t,0}, \tag{9}$$

where $\tau_{t,0}$ is the possible torque preload and $\gamma = \angle(x_c^0 x_c)$ is the rotation of the cam, denoting by $x_c^0$ the axis $x_c$ if $T \equiv B$.

The wire $w$ is kept under tension by a force $f_e$ applied to $E$ and parallel to $x_0$. The so-far described mechanism transforms the translation of $E$ parallel to $x_0$ into a rotation $\gamma$ of the cam.

As depicted in Fig. 6, increasing $f_e$ the length of $w_f$ increases, the cam rotates of an increasing angle $\gamma$ and $T$ slides from $B$ to $A$. Let us denote by $\Delta x_E$ the displacement of

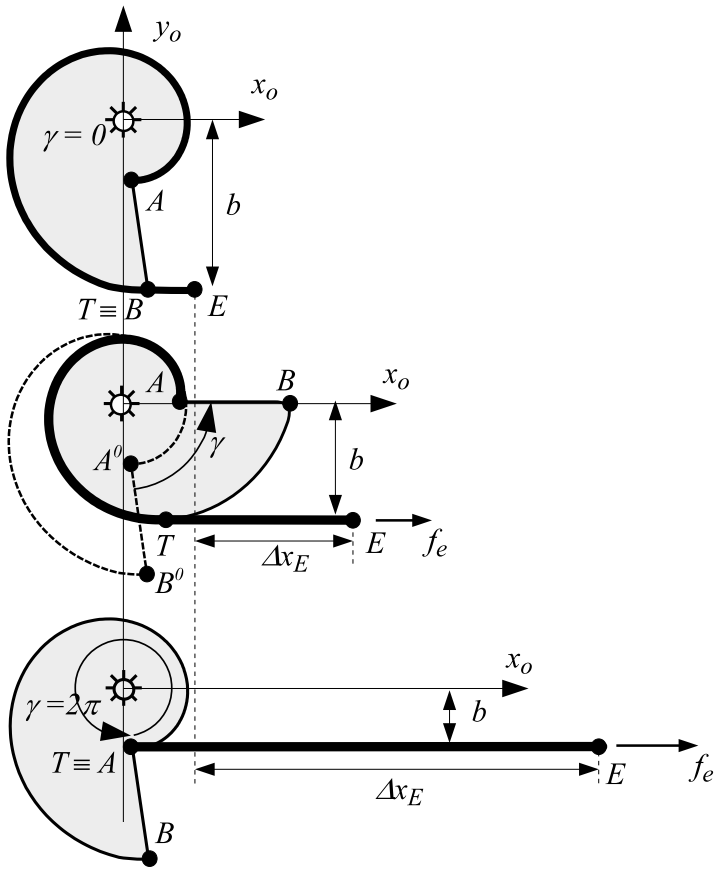


Figure 6: Applying the force $f_e$ to $E$, the wire is more and more unwrapped from $c$ and $T$ "slides" from $B$ to $A$.

$E$ along $x_0$, with respect to the reference configuration in which $T \equiv B$. $\Delta x_E$ denotes also the elongation of the virtual tension spring applied in $E$ along $w_f$, generated by the LinWWC-SEA.

Referring to Fig. 7 and considering the wire inextensibility, the differential translation of $E$ (and $T$) along $f_e$, i.e. the variation of length $w_f$ wrt the cam rotation, is

$$\frac{\mathrm{d}w_f}{\mathrm{d}\gamma} = r\cos\beta \tag{10}$$

Similarly, its normal component, i.e. the differential of $b$ wrt $\gamma$ is

$$\frac{\mathrm{d}b}{\mathrm{d}\gamma} = r\sin\beta \tag{11}$$

Consequently, $w_f$ and $b$ are functions of $\gamma$

$$w_f = \int \frac{\mathrm{d}w_f}{\mathrm{d}\gamma}\,\mathrm{d}\gamma + w_{f,0} \tag{12}$$

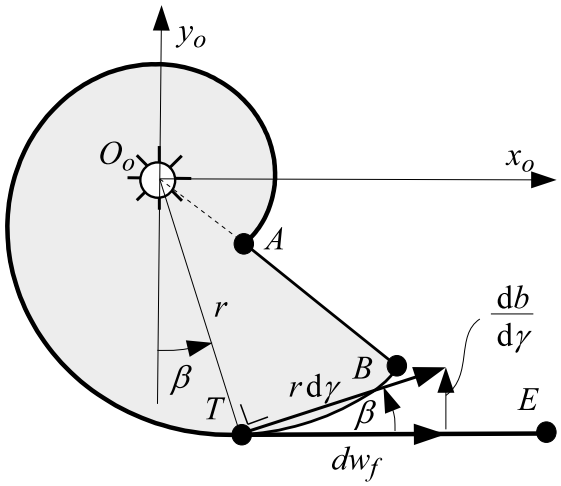


Figure 7: Differential displacement of $T$.

$$b = \int \frac{\mathrm{d}b}{\mathrm{d}\gamma}\,\mathrm{d}\gamma + b_B \tag{13}$$

where $w_{f,0}$ and $b_B$ denotes the values of $w_f$ and $b$, respectively, if $T \equiv B$.

The length of $w_c$ is given by (6).

Given the externally applied force $f_e$, the system is in static equilibrium if

$$\tau_t(\gamma) = f_e b(\gamma). \tag{14}$$

where both $\tau_t$ and $b$ are function of $\gamma$ and can be obtained by (9) and (13), respectively.

The mechanism transforms the torsional stiffness $k_t$ to a virtual extension spring applied to $E$ whose stiffness is

$$k_l = \frac{k_t}{b^2}. \tag{15}$$

In conclusion, in order to realize a virtual tension spring with $k_l$ monotonically increasingly wrt $\theta$ and considering a constant-stiffness (i.e. linear) torsion spring, it is required to profile the cam as a spiral (as previously mentioned), with $r$, and more precisely $b$, monotonically increasingly wrt $\theta$.

However, the so-far considered configuration has a unnegligible drawback: referring to Fig. 6 it is notable that varying the intensity of $f_e$, $E$ does not translate in parallel to $f_e$ and $x_o$ because of the variation of $b$. In order to avoid this, it is convenient to refer to the scheme depicted in Fig. 8, where $w$ partially wraps $c$ and, after detaching from it, is partially wrapped on a circular profile (e.g. a pulley), namely $p$, with radius of curvature $\rho$. The wire $w$ can be ideally split into four parts

- $w_c$ is wrapped on $c$, between $A$ and $T$;
- $w_b$ is between $T$ on $c$ and $U$ on $p$;

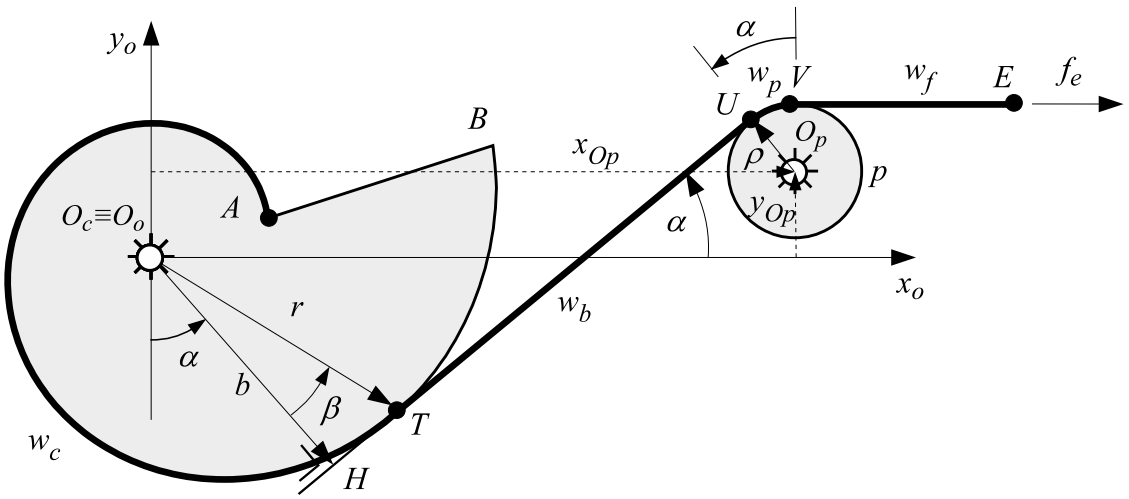


Figure 8: The LinWWC-SEA coupled with a pulley.

- $w_p$ is wrapped on $p$, between $U$ and $V$;
- $w_f$ is between $V$ on $p$ and the free endpoint $E$.

resulting in $w = w_c + w_b + w_p + w_f$. The angle $\alpha$ denotes the inclination of $w_b$ wrt $x_o$. The line $w_b$ is tangent to $c$, tangent to $p$ and passes through $T$.

Given $r(\theta)$, and therefore $b(\theta)$ from (7) and (8), the following geometrical conditions must be respected (refer to Table 1 for symbols):

$$\begin{cases} d(O_c, \overleftrightarrow{TU}) = b \\ d(O_p, \overleftrightarrow{TU}) = \rho \\ T \in w_b \end{cases} \tag{16}$$

Referring to $\{o\}$, given that the Cartesian coordinates of $H(x_H, y_H)$ are $H\,(b\sin\alpha, -b\cos\alpha)$, the generic line passing through $H$ is

$$m(x - x_H) - (y - y_H) = x\tan\alpha - y - \frac{b}{\cos\alpha} = 0, \tag{17}$$

denoting the slope $m = \tan\alpha$.

The condition $d(O_p, \overleftrightarrow{TU}) = \rho$ of (16) can be applied recalling that, as it is well known, the distance $\rho$ between a line in the form $c_1 x + c_2 y + c_3 = 0$ and the point $(x_{O_p}, y_{O_p})$ is

$$\rho = \frac{c_1 x_{O_p} + c_2 y_{O_p} + c_3}{\sqrt{c_1^2 + c_2^2}}, \tag{18}$$

where $c_1 = \tan\alpha$, $c_2 = -1$ and $c_3 = -b/\cos(\alpha)$ from (17).

Therefore, from the previous equation it is possible to obtain the value of $\alpha$ given $\theta$, recalling that $\theta$ is the angular coordinate of the cam profile (Fig. 4).

The endpoints of $w_b$ are

$$T \equiv (x_T, y_T) \equiv (r\sin(\alpha+\beta), -r\cos(\alpha+\beta)) \tag{19}$$

$$U \equiv (x_U, y_U) \equiv \left(-\rho\sin(\alpha) + x_{O_p}, \rho\cos(\alpha) + y_{O_p}\right). \tag{20}$$

Consequently it is

$$w_b = \overline{TU} \tag{21}$$

$$w_p = \rho\angle(VO_pU) = \rho\alpha \tag{22}$$

given that $V$ is the point on $w_f$ at distance $\rho$ from $O_p$, considering that $w_f$ is aligned to $f_e$ and parallel to $x_0$. The other parts of the wire are $w_c$, given by (6), and $w_f$, given by (12).

## 4. LinWWC-VSA

According to the scheme reported in Fig. 2, it is possible to configure two antagonistic LinWWC-SEA to realize a LinWWC-VSA, as depicted in Fig. 9.

In Fig. 10, the LinWWC-VSA is represented in three different configurations, with different values of $\delta$ and $\xi$. Similarly to (5), $\delta = (\Delta x_{E,1} + \Delta x_{E,2})/2$, denoting by $\Delta x_{E,i}$ the elongation of the virtual spring corresponding to the $i$-th RotWWC-SEA, and by $\xi$ the translation of $m$ from the equilibrium configuration.

All the elements are embedded in the carriage and do not affect the overall stroke of the linear carriage, not imposing any inherent limit to the stroke length.

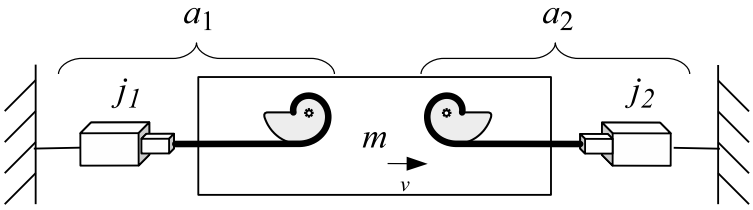


Figure 9: Two antagonistic LinWWC-SEA make up the LinWWC-VSA.

## 5. Synthesis of the cam profile

In this section two different methods, one numerical and one analytic, to design the profile of the cam are presented.

### *5.1. The logarithmic spiral*

The logarithmic spiral is beneficial from the design point of view, since it allows the analytic synthesis of the cam profile in an explicit way. As it is known, it is defined in polar coordinates by

$$r = c_1 e^{c_2\theta}, \tag{23}$$

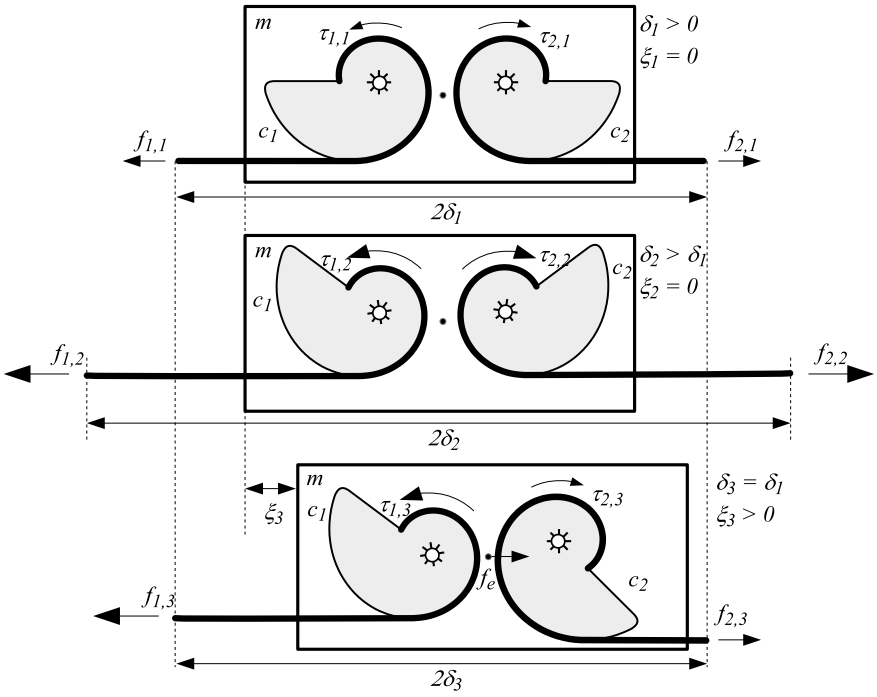


Figure 10: Effect of modifying wire pretensioning and mobile body position.

with $e$ being the base of natural logarithms, and $c_1$ and $c_2$ being arbitrary positive real constants. The logarithmic spiral has the property that the pitch angle $\beta$ is constant.

Let us define the ratio between the maximum and the minimum stiffness of the virtual tension spring applied in $E$ by

$$\Gamma_{kl} = k_{l(A)}/k_{l(B)} \tag{24}$$

where $k_{l(A)}$ and $k_{l(B)}$ denotes $k_l$ if $T \equiv A$ and $T \equiv B$, respectively.

Considering a constant torsional stiffness $k_t$, combining (8), (15) and (24), it is

$$\Gamma_{kl} = \frac{k_t}{(r_A \cos\beta)^2} \frac{(r_B \cos\beta)^2}{k_t} = \left(\frac{r_B}{r_A}\right)^2. \tag{25}$$

leading to

$$\Gamma_{kl} = \left(\frac{c_1 e^{c_2\theta_B}}{c_1 e^{c_2\theta_A}}\right)^2 = \left(e^{c_2(\theta_B-\theta_A)}\right)^2 \Rightarrow c_2 = \frac{\ln(\Gamma_{kl})}{2\Delta\theta}. \tag{26}$$

where $\Delta\theta = \theta_B - \theta_A$. Given the maximum radius of the cam $r_B$ and given the total wrapping angle $\Delta\theta$, it is

$$c_1 = \frac{r_B}{e^{c_2\Delta\theta}}. \tag{27}$$

Therefore, given $\Gamma_{kl}$, $\Delta\theta$ and $r_B$ as design parameters and assuming to use a logarithmic profile, the profile of the cam is completely defined and can be obtained analytically by (26) and (27).

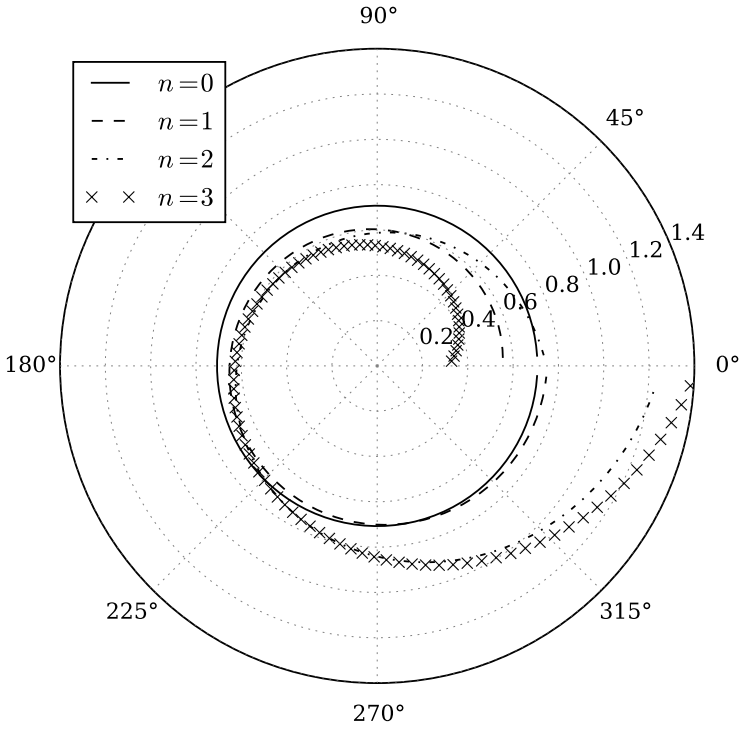


Figure 11: Cam optimized to resemble a quadratic spring.

*5.2. Numerical synthesis*

Let us now focus on the synthesis of a cam given a desired stiffness-displacement characteristic of the tension virtual spring acting in E, i.e. $k_l(\Delta x_E)$.

To this aim the Levenberg-Marquardt algorithm (LMA) [20, 21], which uses the nonlinear least squares to fit a function to a set of target data, can be effectively applied. In order to design the cam, the set of parameters to be optimized must define its shape.

Let us conveniently define the cam profile as

$$r(\theta) = \sum_{i=0}^{n} a_i \theta^i, \tag{28}$$

where $a_i$ are real constants and $n$ is the degree of the polynomial.

Let us consider $\hat{\Delta X}_E$ and $\hat{K}_l$, sets of target data $\Delta x_E$ and $k_l$, respectively. As previously described, both of them depend explicitly on $\theta$. Therefore, the function optimized by LMA evaluates $\Delta x_E$ and $k_l$ as function of $\theta$. It is worth to note that, since the LMA finds only a local minimum, as many fitting algorithms, which is not necessarily the global minimum, it is necessary to specify reasonable starting parameters.

By way of example, the routine has been used to design a LinWWC-SEA with a quadratic force-displacement characteristic, i.e. a linear stiffness-displacement characteristic. It is

worth to note that quadratic springs are often looked for in VSAs since they allow to decouple position and stiffness control [4]. Hereafter the routine is applied to find the $a_i$ parameters of (28), comparing results for different degrees of the polynomial with $0 \leq n \leq 3$. The target set of values is

$$\Delta x_E = \{1, 1.5, 2, 2.5, 3\}\,\mathrm{m}, \qquad k_l = \Delta x_E \mathrm{N\,m^{-2}}, \qquad f_e \propto (\Delta x_E)^2 \tag{29}$$

considering a torsional spring $k_t = 1\,\mathrm{N\,m\,rad^{-1}}$ and considering a LinWWC-SEA without any pulley $p$.

The resultant polynomial expressions are reported in Table 2 as function of $n$. The graphic representations of the optimized cams are reported in Fig. 11. The actual stiffness-displacement curves of the cams are reported in Fig. 12, together with target values.

Table 2: Parameters of the optimized cam.

| n | $r(\theta)$ |
|---|---|
| 0 | $0.707$ |
| 1 | $0.031\theta + 0.554$ |
| 2 | $0.039\theta^2 - 0.162\theta + 0.747$ |
| 3 | $0.010\theta^3 - 0.071\theta^2 + 0.224\theta + 0.315$ |

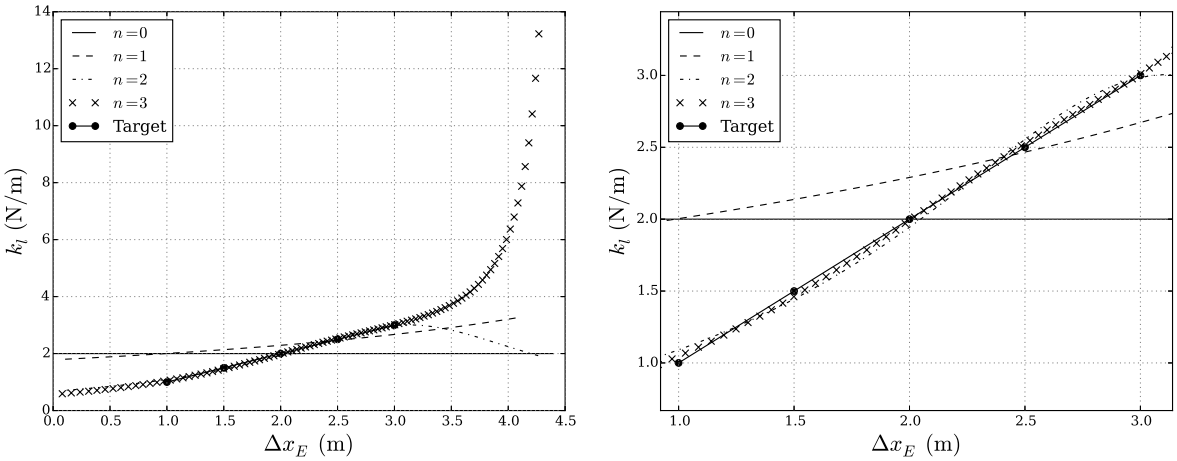


Figure 12: Stiffness-displacement curve of the optimized cam, as function of the order of the polynomial to be optimized. On the right a detailed view of the target characteristic.

## 6. Analysis of the LinWWC-VSA and discussion

Let us now consider an example to analyze the behavior of a LinWWC-VSA applying the presented equations. The considered LinWWC-VSA is made up of two antagonist LinWWC-SEA configured with the parameters reported in Table 3 with a cam shaped as a logarithmic

Table 3: Parameters of a LinWWC-SEA with a logarithmic spiral.

| Parameter | Description | Value | Unit |
|---|---|---|---|
| $\Gamma_{kl}$ | Ratio between maximum and minimum stiffness | 10 | – |
| $r_B$ | Maximum radius of the cam | 1 | m |
| $\Delta\theta$ | Angular extension of the cam | $2\pi$ | rad |
| $c_1$ | Constant of the logarithmic spiral | 0.316227 | m |
| $c_2$ | Constant of the logarithmic spiral | 0.183236 | $\mathrm{rad}^{-1}$ |
| $\rho$ | Radius of pulley $p$ | 0.1 | m |
| $[x_{Op}, x_{Op}]$ | Position of pulley $p$ | $[1.1, -0.1]$ | m |
| $k_t$ | Stiffness of the torsion spring | 1 | $\mathrm{N\,m\,rad}^{-1}$ |

spiral. The apparently questionable unit values of $r_B = 1\,\mathrm{m}$ and $k_t = 1\,\mathrm{N\,m\,rad}^{-1}$, which represent a relatively big cam and compliant torsion spring if compared to typical geometric and stiffness data characterizing mechatronic solutions, have been adopted as normalized values. In fact, the numerical results illustrated hereafter can be straightforwardly applied for other values of $r_B$ and $k_t$ taking into account that

$$\Delta x_E, \xi, \delta \propto r_B; \qquad \tau \propto k_t; \qquad f, f_a \propto \frac{1}{r_B^2}; \qquad k_l, k_a \propto \frac{k_t}{r_B^2}. \tag{30}$$

The effects of including or not including the deflecting pulley $p$ depicted in Fig. 8 are highlighted. Parameters $c_1$ and $c_2$ have been evaluated applying (26) and (27), given $\Gamma_{kl}$, $r_B$ and $\Delta\theta$.

A simulation of the LinWWC-SEA as function of different values of $\theta_T$ is represented in Fig. 13. As $T$ moves from $B$ to $A$ along the cam, the length of the free wire $w_f$ and the rotation $\gamma$ increase. It is notable the effect of the pulley $p$ which keeps constant the vertical coordinate of $E$ but which influences the inclination $\alpha$.

Numerical results reported hereafter refer both to the configuration with and without the pulley $p$ (Fig. 14) which, as better detailed later, affects the total exploitable rotation angle $\gamma$.

The kinematic relationship between $\Delta x_E$, i.e. the elongation of the tension virtual spring, and the rotation of the cam $\gamma$ is represented in Fig. 15. It is notable how the pulley $p$ affects the overall exploitable displacement of $E$, keeping constant the shape of the cam. This results in a virtual spring with a shorter maximum elongation.

In Fig. 16 the two stiffnesses of the mechanism are represented. The torsional stiffness $k_t$ is the same reported in Table 3 and is independent on $\Delta x_E$, as expected. The non-linear stiffness $k_l$ of the virtual tension spring applied in $E$ is determined by the actual shape of the cam and is also influenced by the presence of the pulley $p$. The ratio between the maximum and the minimum stiffness $\Gamma_{kl}$ is due to the cam profile and is obtained applying (26) and (27), independently from the presence of the pulley since $k_l$ depends only on $k_t$ and $b$ (see (15)). On the other side, its presence influences the slope of the curve because of the shorter overall displacement of $E$, as previously said about Fig. 15.

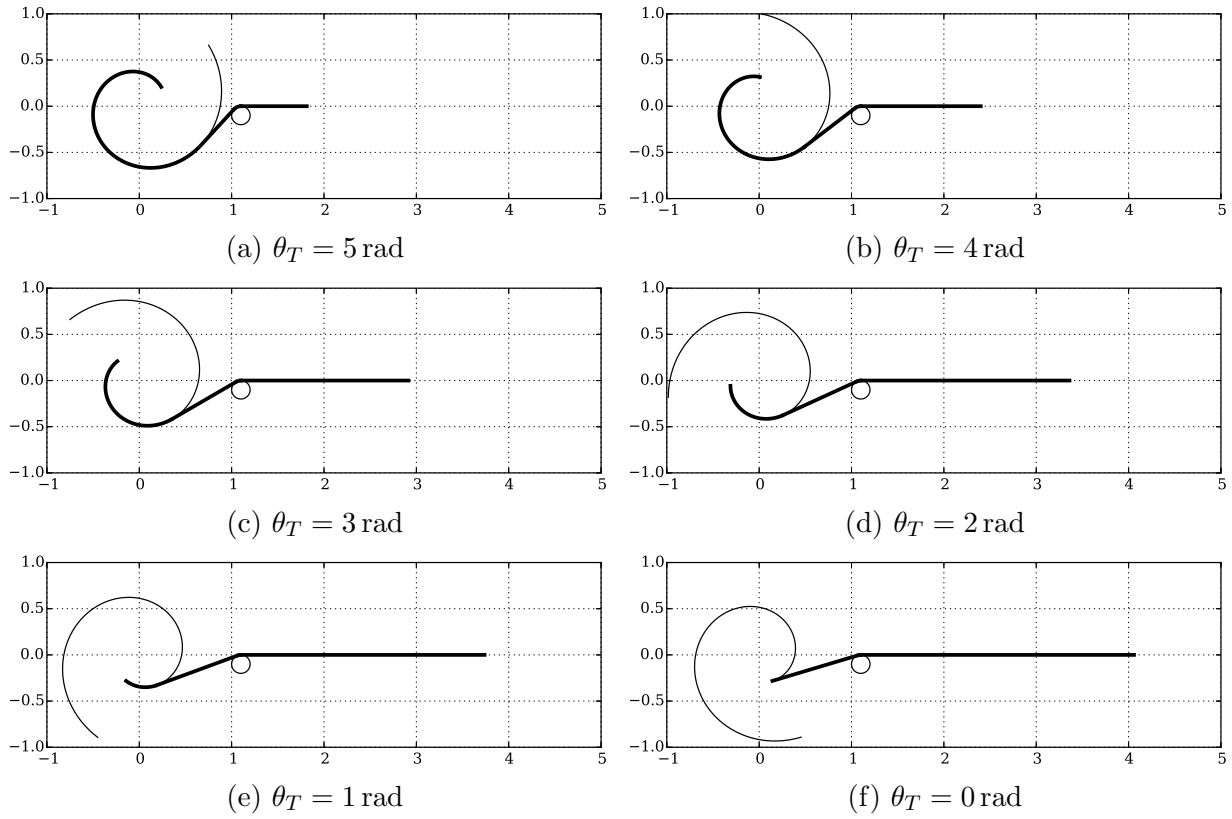

(a) $\theta_T = 5\,\text{rad}$ (b) $\theta_T = 4\,\text{rad}$

(c) $\theta_T = 3\,\text{rad}$ (d) $\theta_T = 2\,\text{rad}$

(e) $\theta_T = 1\,\text{rad}$ (f) $\theta_T = 0\,\text{rad}$

Figure 13: Kinematic simulation of wire-unwrapping in LinWWC-SEA, from a) to f).

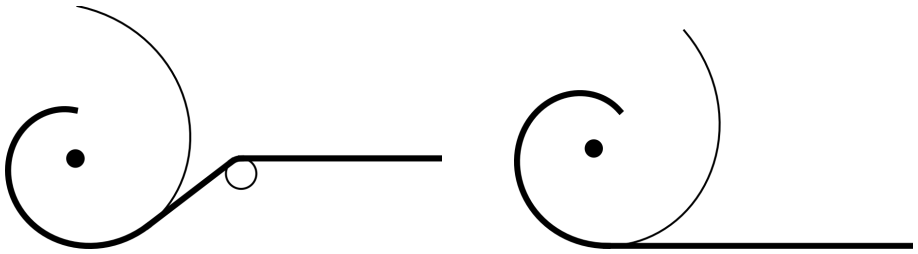

(a) Cam with pulley. (b) Cam without pulley.

Figure 14: Cam with and without pulley $p$.

The torque and force exerted by the torsion spring and by the virtual tension spring are represented in Fig. 17. It is worth to underline that the maximum tension force exerted by the wire is reduced by the presence of the pulley, because of the reduced maximum displacement of $E$.

Let us now refer to LinWWC-VSA, i.e. the coupled effect of two antagonistic LinWWC-SEA. The surfaces representing the force applied to and the stiffness of the mobile body $m$, as function of $\delta$ and $\xi$ are represented in Fig. 18. Both $f_a$ and $k_a$ grow with the growth of $\delta$, keeping $\xi$ constant. The maximum value of $f_a$ is achieved with the highest value of

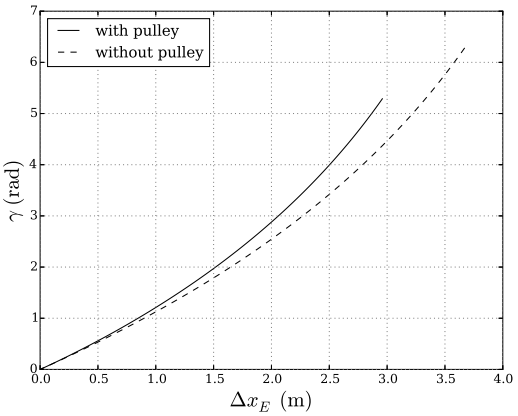


Figure 15: Rotation of the cam $\gamma$ as function of the extension $\Delta x_E$ of the virtual spring applied in $E$.

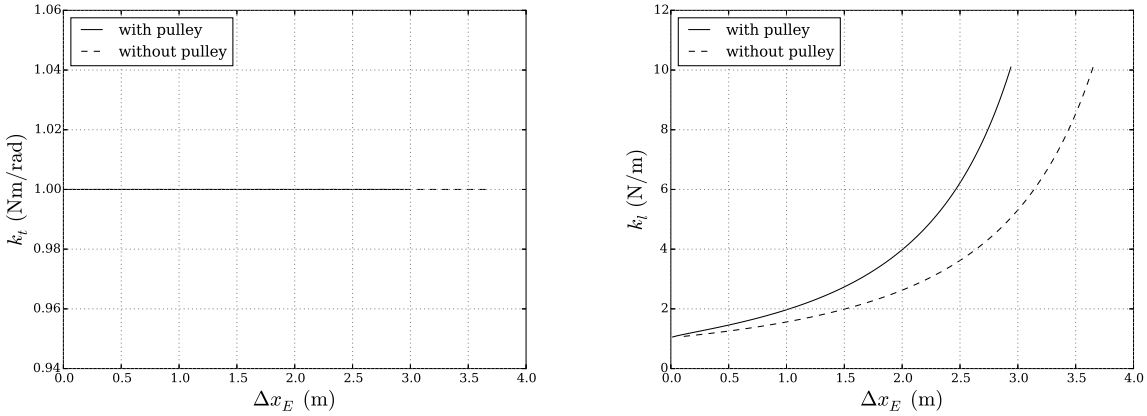


(a) Stiffness of the torsion spring.

(b) Tensional stiffness of the wire in $E$.

Figure 16: Stiffnesses as function of the extension $\Delta x_E$. (a) As reported in Table 3, $k_t$ is constant and independent of $\Delta x_E$. (b) The stiffness non-linearity of the virtual spring $k_l$ applied in $E$, required to realize a VSA and obtainable by the cam-based transmission mechanism, is notable.

$\xi$, with $\delta = \xi$. The maximum value of $k_a$ is achieved with the highest value of $\delta$ with $\xi = 0$. The maximum theoretical stiffness cannot therefore be exploited moving $m$ from its equilibrium position. Zero values of $f_a$ and $k_a$ refer to not allowed configurations. In fact, it is notable the main drawback of this type of actuator: the actually exploitable range of motion of $m$ depends on $\delta$. The limits of $\xi$ are due to the fact that the two LinWWC-SEA reach their endstrokes (i.e. $T \equiv A$ or $T \equiv B$) independently and according to their actual values of $\Delta x_E$. The maximum and the minimum stiffness of LinWWC-VSA are therefore not exploitable configurations, in the sense that no displacement of $m$ is allowed.

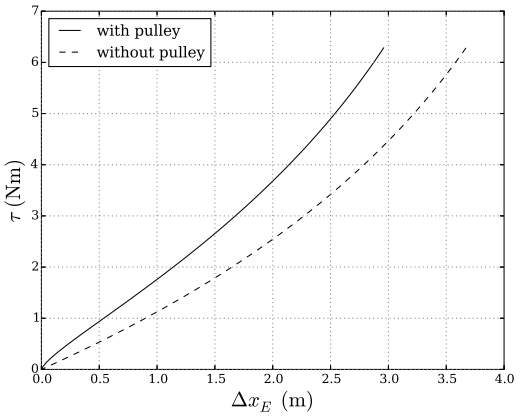


(a) Torque exerted by the torsion spring.

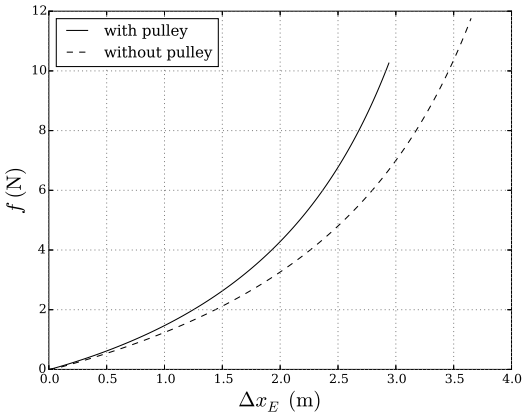


(b) Tension force exerted to the wire in $E$.

Figure 17: Force and torque as function of the extension $\Delta x_E$ of the virtual spring applied in $E$.

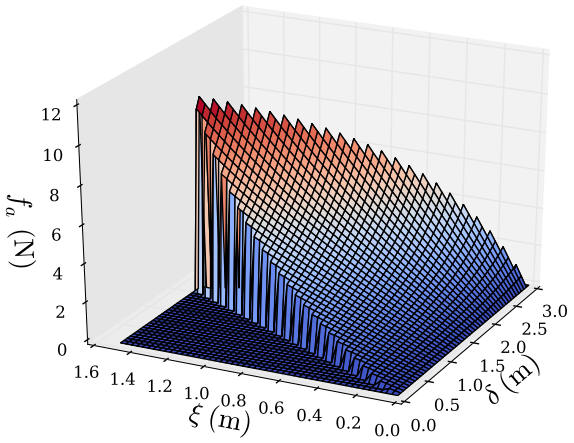


(a) Force on $m$.

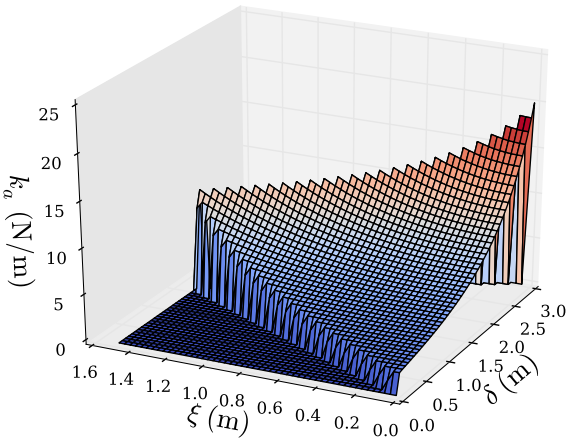


(b) Stiffness of $m$.

Figure 18: Force and stiffness of the mobile body $m$ as function of $\delta$ and $\xi$.

## 7. Conclusions

The LinWWC-VSA is an agonist-antagonist variable stiffness actuation scheme specifically conceived for linear motions. It is characterized by a relatively simple set of components and does not require strict manufacturing tolerances. The cam profile can be designed according to the required specifications of the applications, with both numerical and analytical methods. The compliant actuation scheme can be embedded in pre-existing linear carriages. Two concept designs of mobile carriages embedding the LinWWC-VSA are depicted in Fig. 19. The coaxial configuration (Fig. 19b) is embedded as actuation scheme of a variable stiffness device for upper-limb rehabilitation (Fig. 20), improved version of the previously developed device described in [22]. In order to reduce the overall dimensions of

the cams, it is possible to profile them as multiple-turns spiral cams (Fig. 21). As depicted in Fig. 22, two LinWWC-VSA can be configured orthogonally to realize a 2-DOF planar mobile element guaranteeing planar tension forces.

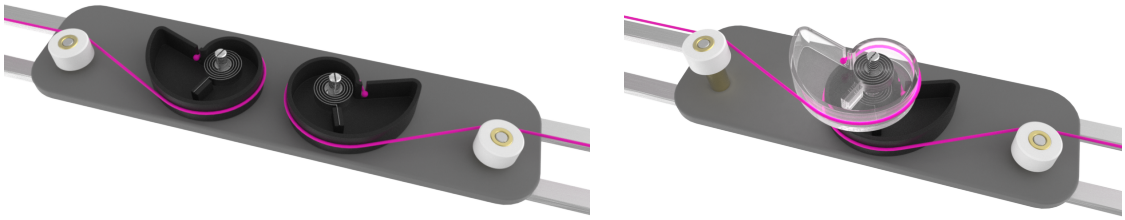

(a) Coplanar configuration. (b) Coaxial configuration.

Figure 19: Two concept designs of linear carriages embedding the LinWWC-VSA. (a) Coplanar configuration with wires lying on the same plane. (b) Coaxial configuration with cams pivoting around the same shaft. The latter has the advantage of being more compact; on the other side, it generates a torque on the carriage due to the offset between the planes of the two wires.

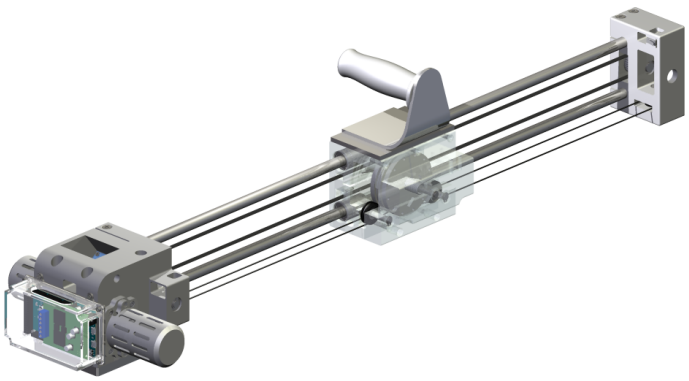

Figure 20: LINarm2: a variable stiffness device for upper-limb rehabilitation embedding the LinWWC-VSA architecture with the coaxial configuration (Fig. 19b).

## Acknowledgments

The authors would like to thank João Carlos Dalberto and Roberto Bozzi for the support to the mechanical design and the realization of the LINarm2 prototype.

This work was supported by the European Union [grant agreement no FP7-ICT-601116].

Figure 21: A multiple-turns spiral cam can increase the exploitable wire stroke reducing the overall dimensions of the cam.

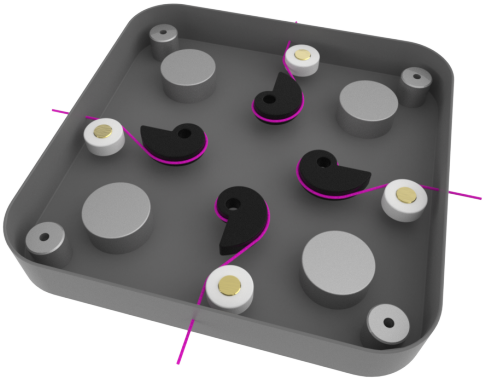

Figure 22: Two LinWWC-VSA can be configured orthogonally to realize a 2-DOF planar mobile element.

## References


[1] B. Vanderborght, A. Albu-Schaeffer, A. Bicchi, E. Burdet, D. G. Caldwell, R. Carloni, M. Catalano, O. Eiberger, W. Friedl, G. Ganesh, M. Garabini, M. Grebenstein, G. Grioli, S. Haddadin, H. Hoppner, A. Jafari, M. Laffranchi, D. Lefeber, F. Petit, S. Stramigioli, N. Tsagarakis, M. Van Damme, R. Van Ham, L. C. Visser, and S. Wolf, "Variable impedance actuators: A review," *Robot. Auton. Syst.*, vol. 61, no. 12, pp. 1601–1614, Dec. 2013. doi: 10.1016/j.robot.2013.06.009

[2] G. Pratt and M. Williamson, "Series Elastic Actuators," in *Intelligent Robots and Systems 95. 'Human Robot Interaction and Cooperative Robots', Proceedings. 1995 IEEE/RSJ International Conference on*, vol. 1, Aug. 1995. doi: 10.1109/IROS.1995.525827 pp. 399–406.

[3] K. Laurin-Kovitz, J. Colgate, and S. Carnes, "Design of components for programmable passive impedance," in *Robotics and Automation, 1991. Proceedings., 1991 IEEE International Conference on*, Apr 1991. doi: 10.1109/ROBOT.1991.131824 pp. 1476–1481 vol.2.

[4] A. Jafari, "Coupling between the output force and stiffness in different variable stiffness actuators," *Actuators*, vol. 3, no. 3, p. 270, 2014.

[5] R. Ham, T. Sugar, B. Vanderborght, K. Hollander, and D. Lefeber, "Compliant actuator designs," *Robotics Automation Magazine, IEEE*, vol. 16, no. 3, pp. 81–94, September 2009. doi: 10.1109/MRA.2009.933629

[6] S. Wolf, G. Grioli, W. Friedl, M. Grebenstein, H. Hoeppner, E. Burdet, D. Caldwell, A. Bicchi, S. Stramigioli, and B. Vanderborght, "Variable stiffness actuators: Review on design and components," *Mechatronics, IEEE/ASME Transactions on*, vol. PP, no. 99, pp. 1–1, 2015. doi: 10.1109/TMECH.2015.2501019

[7] G. Grioli, S. Wolf, M. Garabini, M. Catalano, E. Burdet, D. Caldwell, R. Carloni, W. Friedl, M. Grebenstein, M. Laffranchi, D. Lefeber, S. Stramigioli, N. Tsagarakis, M. Van Damme, B. Vanderborght, A. Albu-Schaeffer, and A. Bicchi, "Variable stiffness actuators: The user's point of view," *Int. J. Rob. Res.*, vol. 34, no. 6, pp. 727–743, May 2015.

[8] "Compliant actuation of parallel-type variable stiffness actuator based on antagonistic actuation," *Journal of Mechanical Science and Technology*, vol. 24, no. 11, 2010. doi: 10.1007/s12206-010-0813-6

[9] G. Tonietti, R. Schiavi, and A. Bicchi, "Design and control of a variable stiffness actuator for safe and fast physical human/robot interaction," in *Robotics and Automation, 2005. ICRA 2005. Proceedings of the 2005 IEEE International Conference on*, April 2005. doi: 10.1109/ROBOT.2005.1570172 pp. 526–531.

[10] N. Tsagarakis, I. Sardellitti, and D. Caldwell, "A new variable stiffness actuator (compact-vsa): Design and modelling," in *Intelligent Robots and Systems (IROS), 2011 IEEE/RSJ International Conference on*, Sept 2011. doi: 10.1109/IROS.2011.6095006. ISSN 2153-0858 pp. 378–383.

[11] S. Groothuis, G. Rusticelli, A. Zucchelli, S. Stramigioli, and R. Carloni, "The variable stiffness actuator vsaut-ii: Mechanical design, modeling, and identification," *Mechatronics, IEEE/ASME Transactions on*, vol. 19, no. 2, pp. 589–597, April 2014. doi: 10.1109/TMECH.2013.2251894

[12] S. Wolf and G. Hirzinger, "A new variable stiffness design: Matching requirements of the next robot generation," in *Robotics and Automation, 2008. ICRA 2008. IEEE International Conference on*, May 2008. doi: 10.1109/ROBOT.2008.4543452. ISSN 1050-4729 pp. 1741–1746.

[13] J. Guo and G. Tian, "Conceptual design and analysis of four types of variable stiffness actuators based on spring pretension," *Int J Adv Robot Syst*, vol. 12, no. 62, 2015. doi: 10.5772/60580

[14] J. Hurst, J. Chestnutt, and A. Rizzi, "The actuator with mechanically adjustable series compliance," *Robotics, IEEE Transactions on*, vol. 26, no. 4, pp. 597–606, Aug 2010. doi: 10.1109/TRO.2010.2052398

[15] B. Vanderborght, N. G. Tsagarakis, R. Ham, I. Thorson, and D. G. Caldwell, "Maccepa 2.0: Compliant actuator used for energy efficient hopping robot chobino1d," *Auton. Robots*, vol. 31, no. 1, pp. 55–65, Jul. 2011.

[16] L. Fiorio, A. Parmiggiani, B. Berret, G. Sandini, and F. Nori, "pnrvsa: human-like actuator with non-linear springs in agonist-antagonist configuration," in *Humanoid Robots (Humanoids), 2012 12th IEEE-RAS International Conference on*, Nov 2012. doi: 10.1109/HUMANOIDS.2012.6651566. ISSN 2164-0572 pp. 502–507.

[17] D. Shin, X. Yeh, and O. Khatib, "Variable radius pulley design methodology for pneumatic artificial muscle-based antagonistic actuation systems," in *Intelligent Robots and Systems (IROS), 2011 IEEE/RSJ International Conference on*, Sept 2011. doi: 10.1109/IROS.2011.6095180. ISSN 2153-0858 pp. 1830–1835.

[18] A. Schepelmann, K. Geberth, and H. Geyer, "Compact nonlinear springs with user defined torque-deflection profiles for series elastic actuators," in *Robotics and Automation (ICRA), 2014 IEEE International Conference on*, May 2014. doi: 10.1109/ICRA.2014.6907350 pp. 3411–3416.

[19] N. Hogan, "Adaptive control of mechanical impedance by coactivation of antagonist muscles," *Automatic Control, IEEE Transactions on*, vol. 29, no. 8, pp. 681–690, Aug 1984. doi: 10.1109/TAC.1984.1103644

[20] K. Levenberg, "A method for the solution of certain non-linear problems in least squares," *Quart. J. Appl. Maths.*, vol. II, no. 2, pp. 164–168, 1944.

[21] D. W. Marquardt, "An algorithm for least-squares estimation of nonlinear parameters," *Journal of the Society for Industrial and Applied Mathematics*, vol. 11, no. 2, pp. 431–441, 1963. doi: 10.1137/0111030

[22] M. Malosio, M. Caimmi, G. Legnani, and L. Tosatti, "Linarm: a low-cost variable stiffness device for upper-limb rehabilitation," in *Intelligent Robots and Systems (IROS 2014), 2014 IEEE/RSJ International Conference on*, Sept 2014. doi: 10.1109/IROS.2014.6943066 pp. 3598–3603.

sea_model.eps

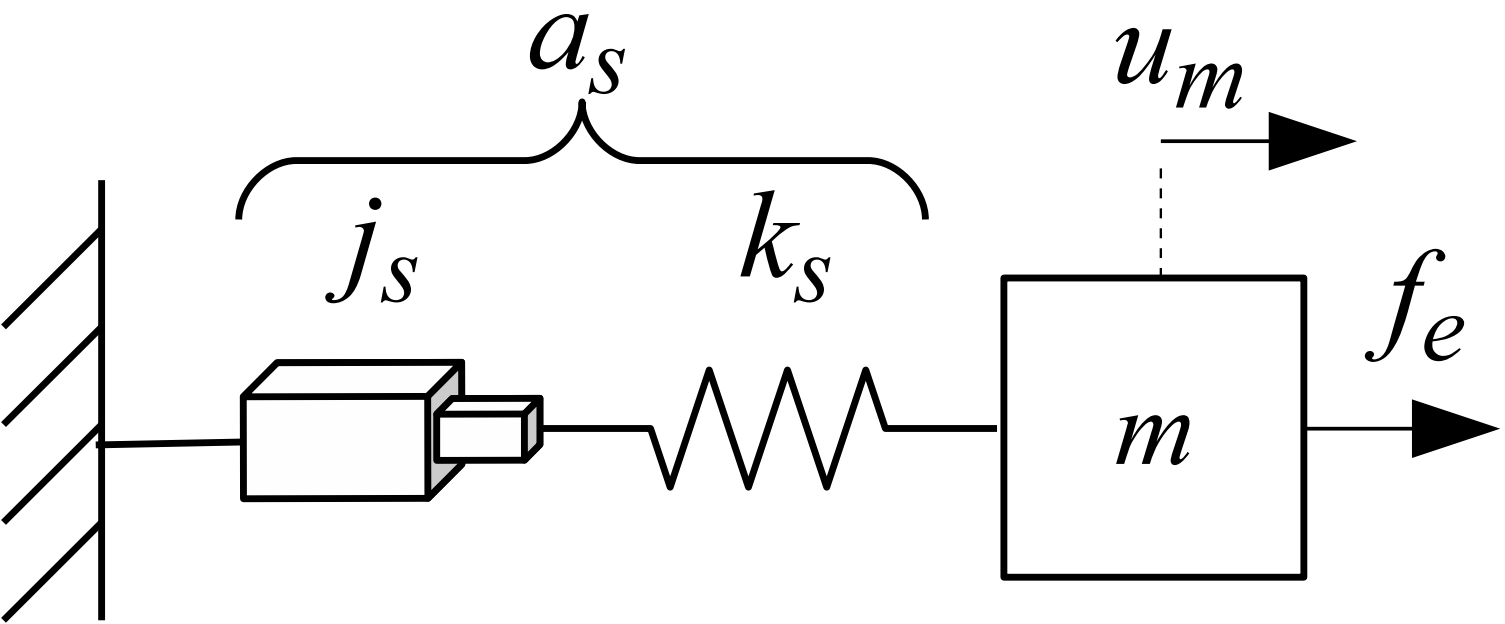

vsa_model.eps

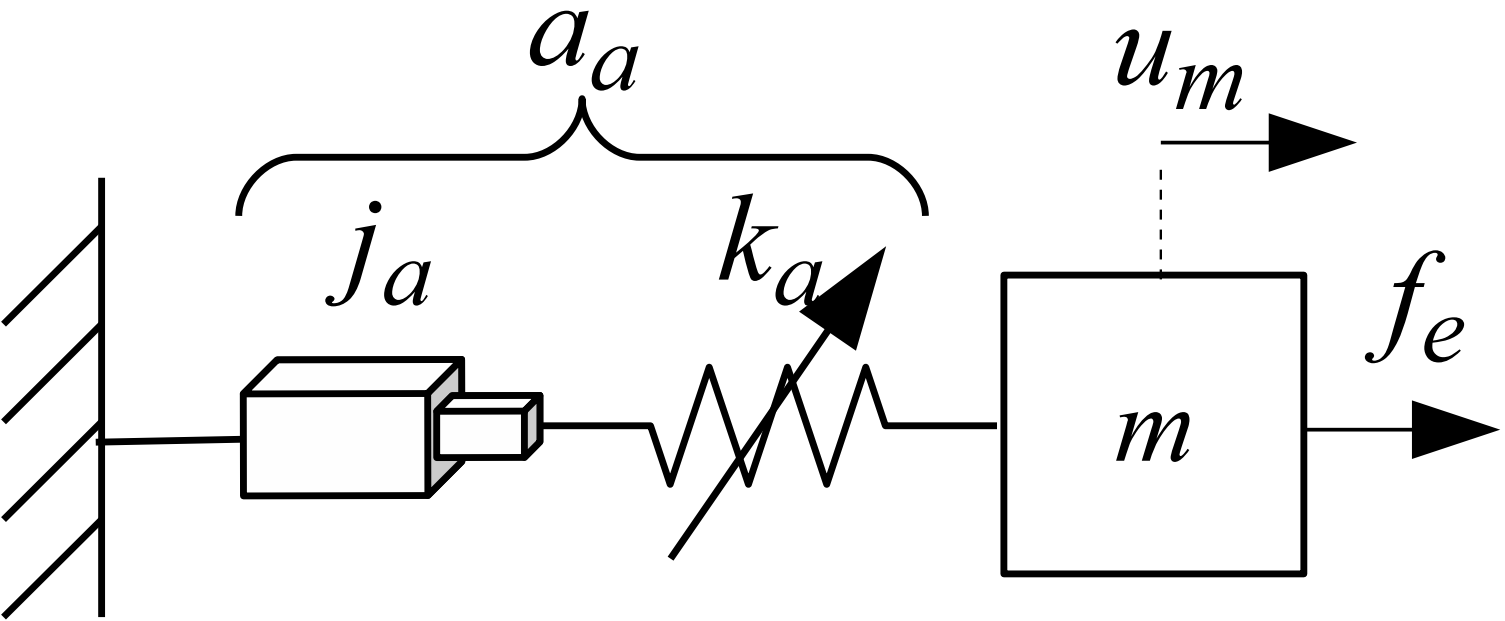

vsa.eps

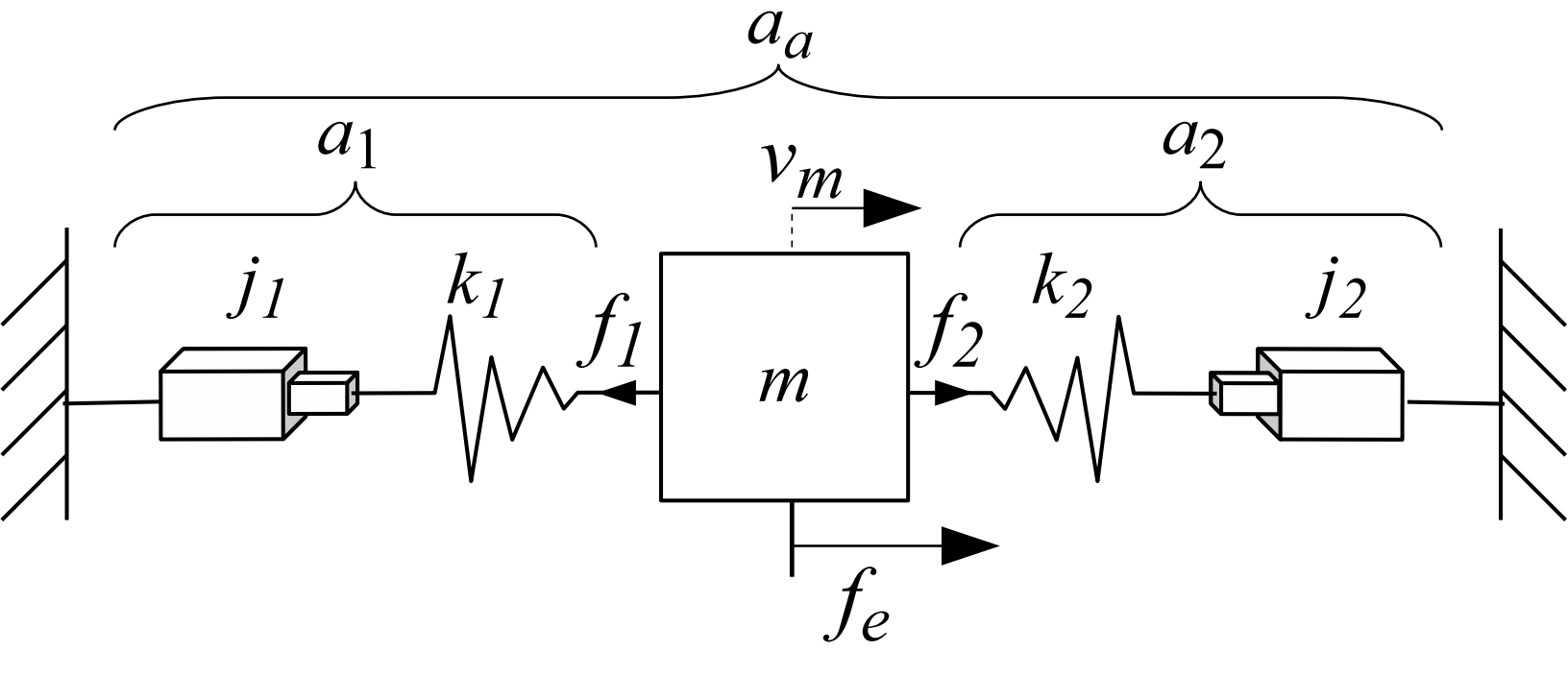

force_vs_u_ant_vsa_graph.eps
$f_1$
$f_2$
$v_e$
$v$
$k_1$
$k_2$
$f_e$
$f_1$
$f_2$
$v_1$
$v_m$
$v_2$
$v$
$k_1$
$k_2$
$\xi$
$\delta$
$f$
$f_2$
$v_1$
$v_e$
$v_m$
$v_2$
$v$
$-f_e$
$f_a$
$f_1$

cam_profile.eps

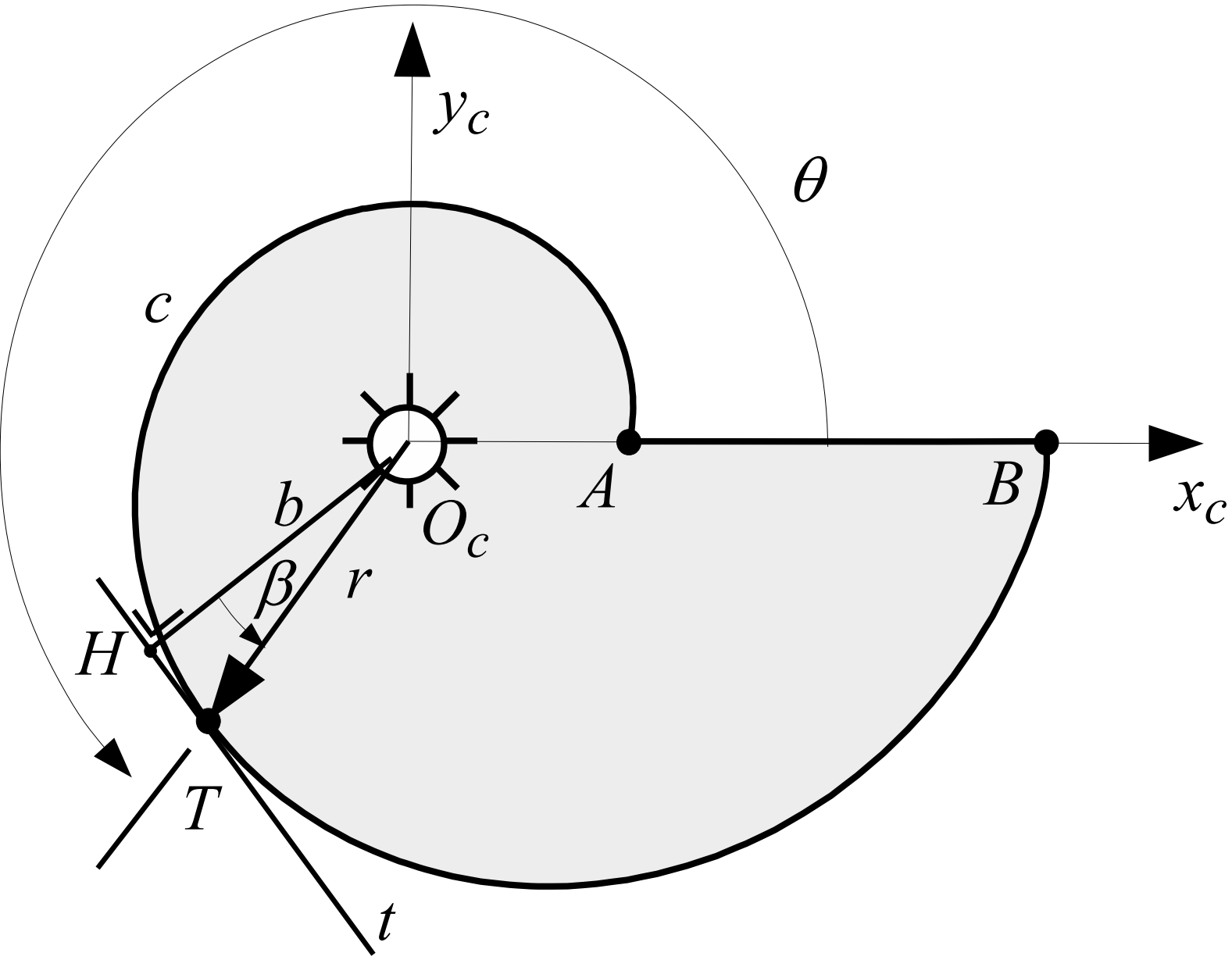

wrapped_cam_spring.eps

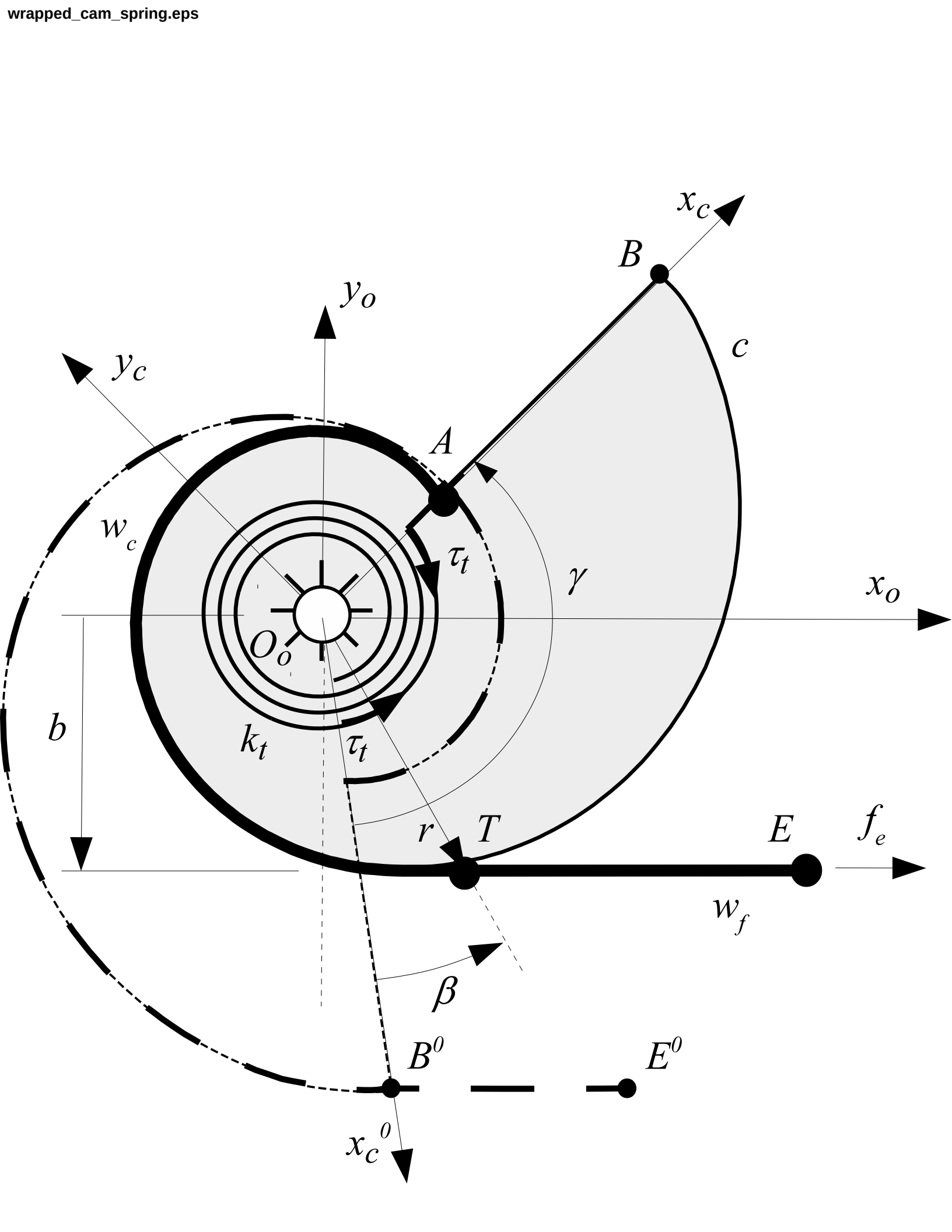

unwrapping_wire.eps

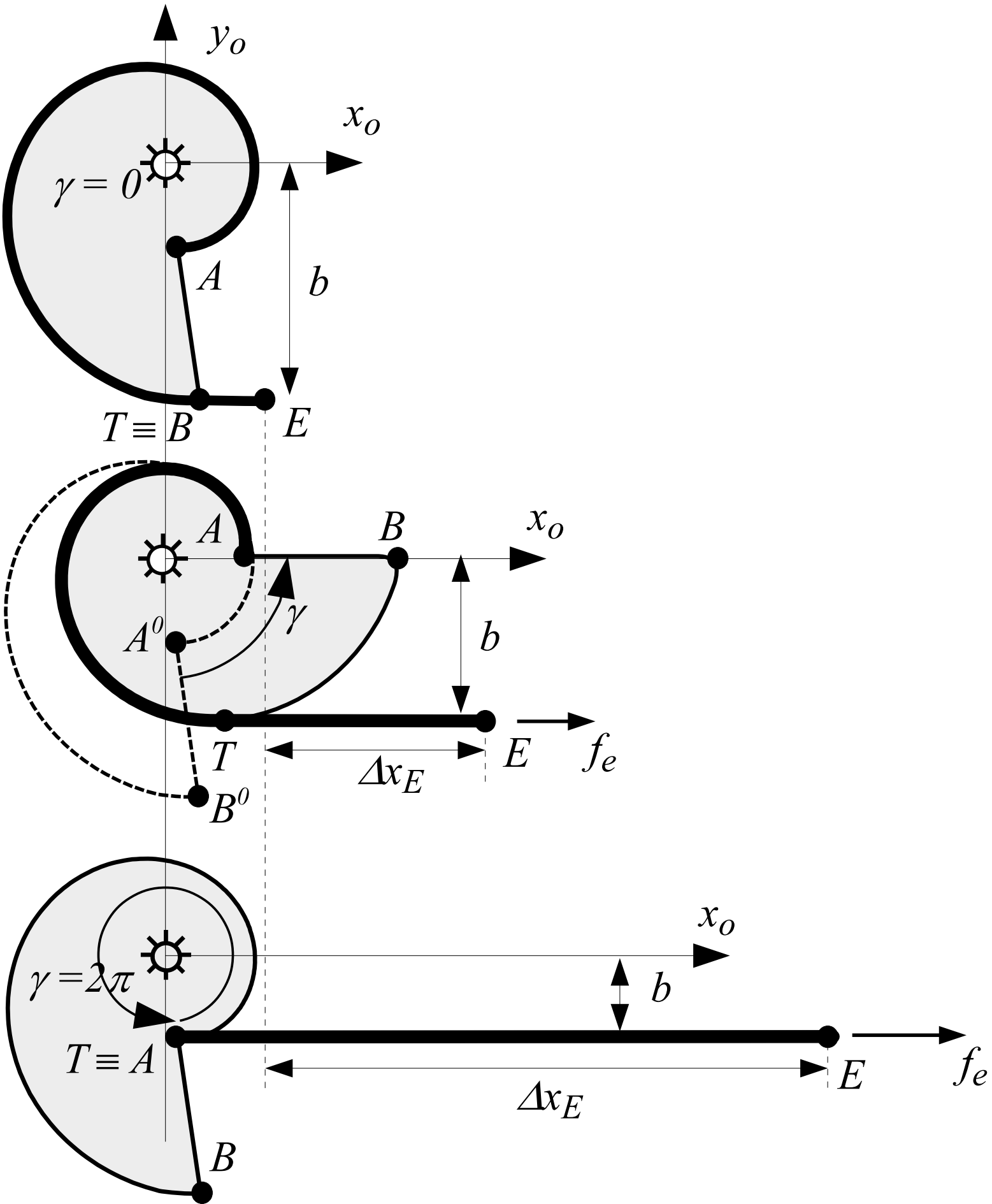

wrapped_cam_theta_gamma.eps

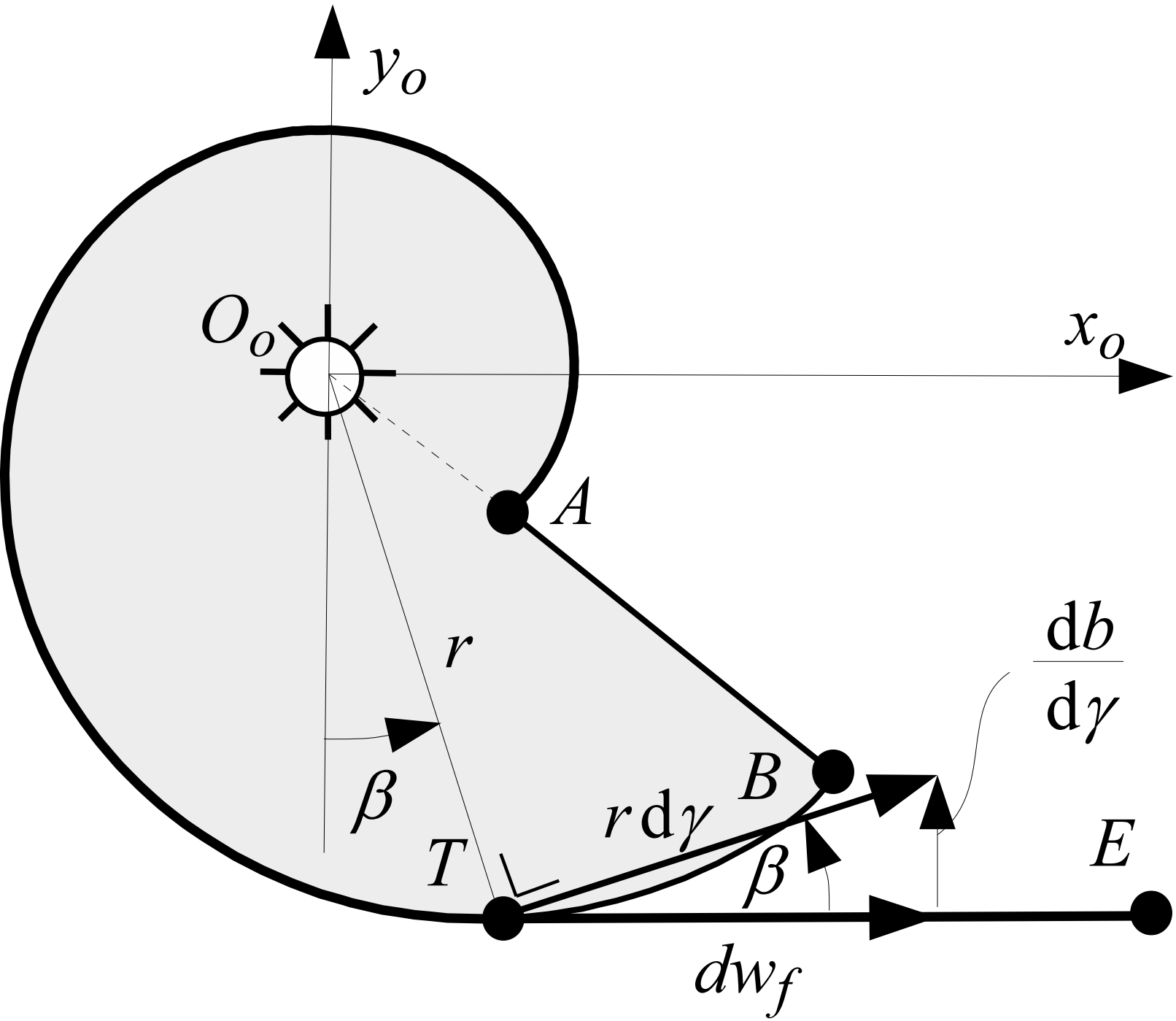

pulleyed-LWWC-SEA.eps

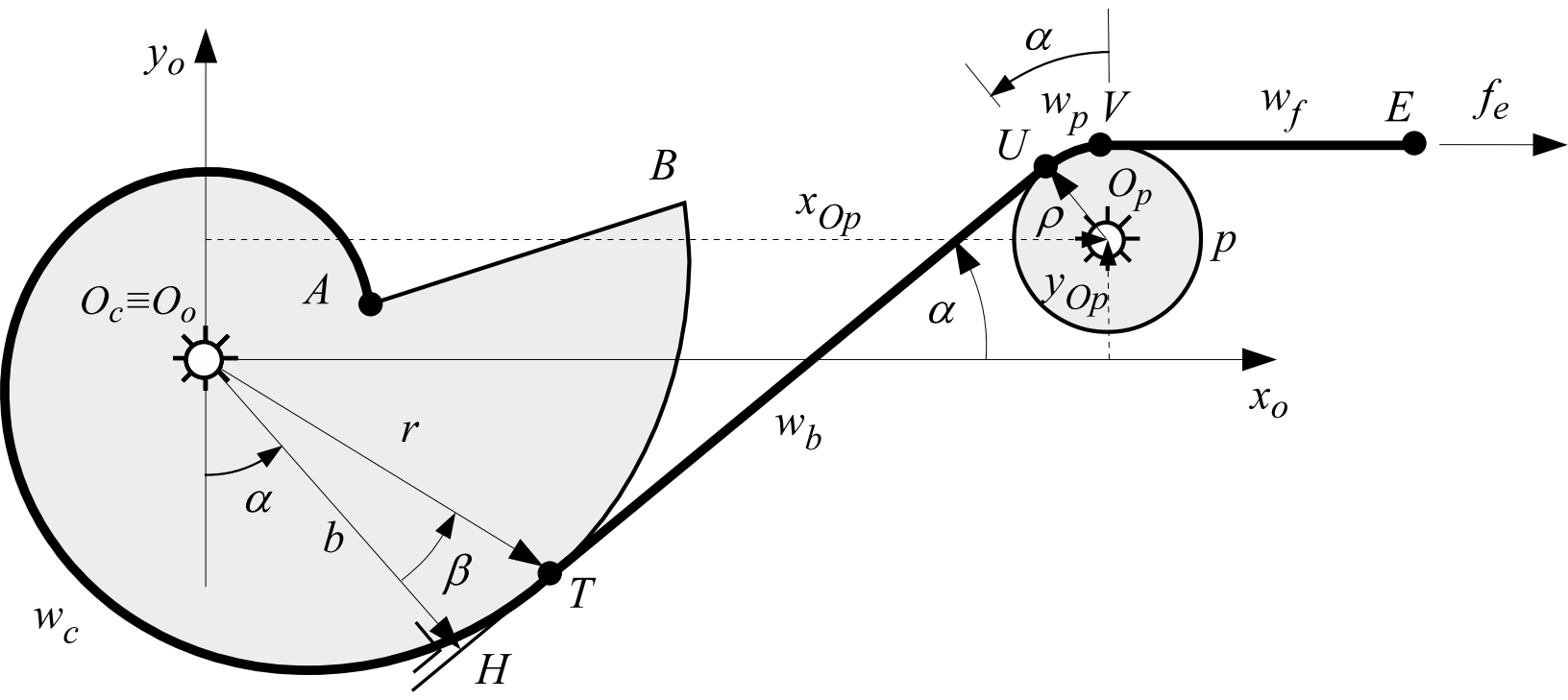

LWWC-VSA.eps

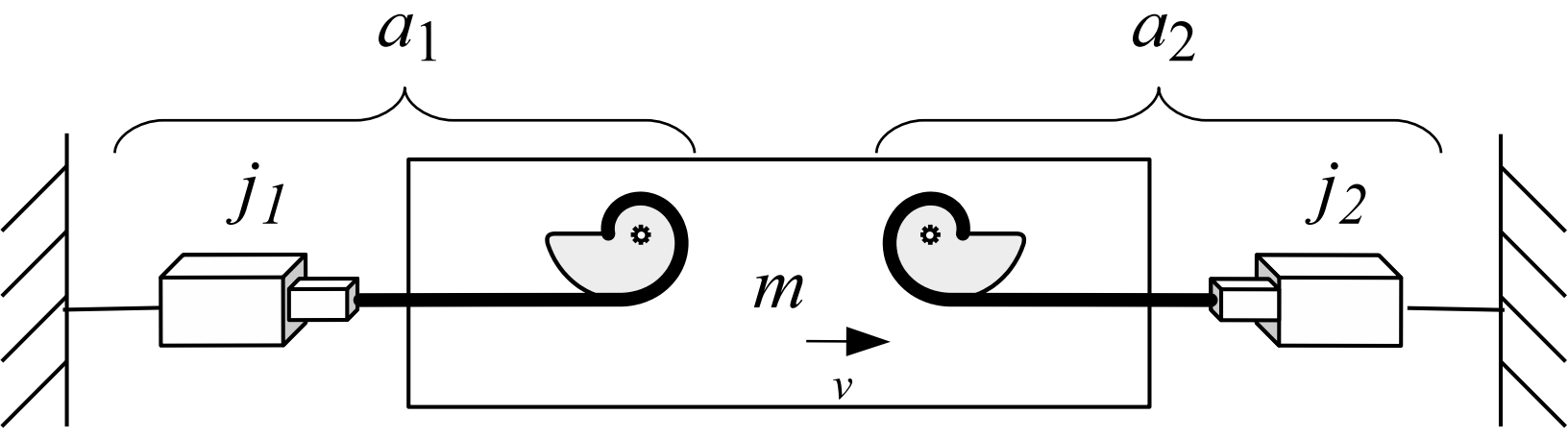

cam_preload.eps

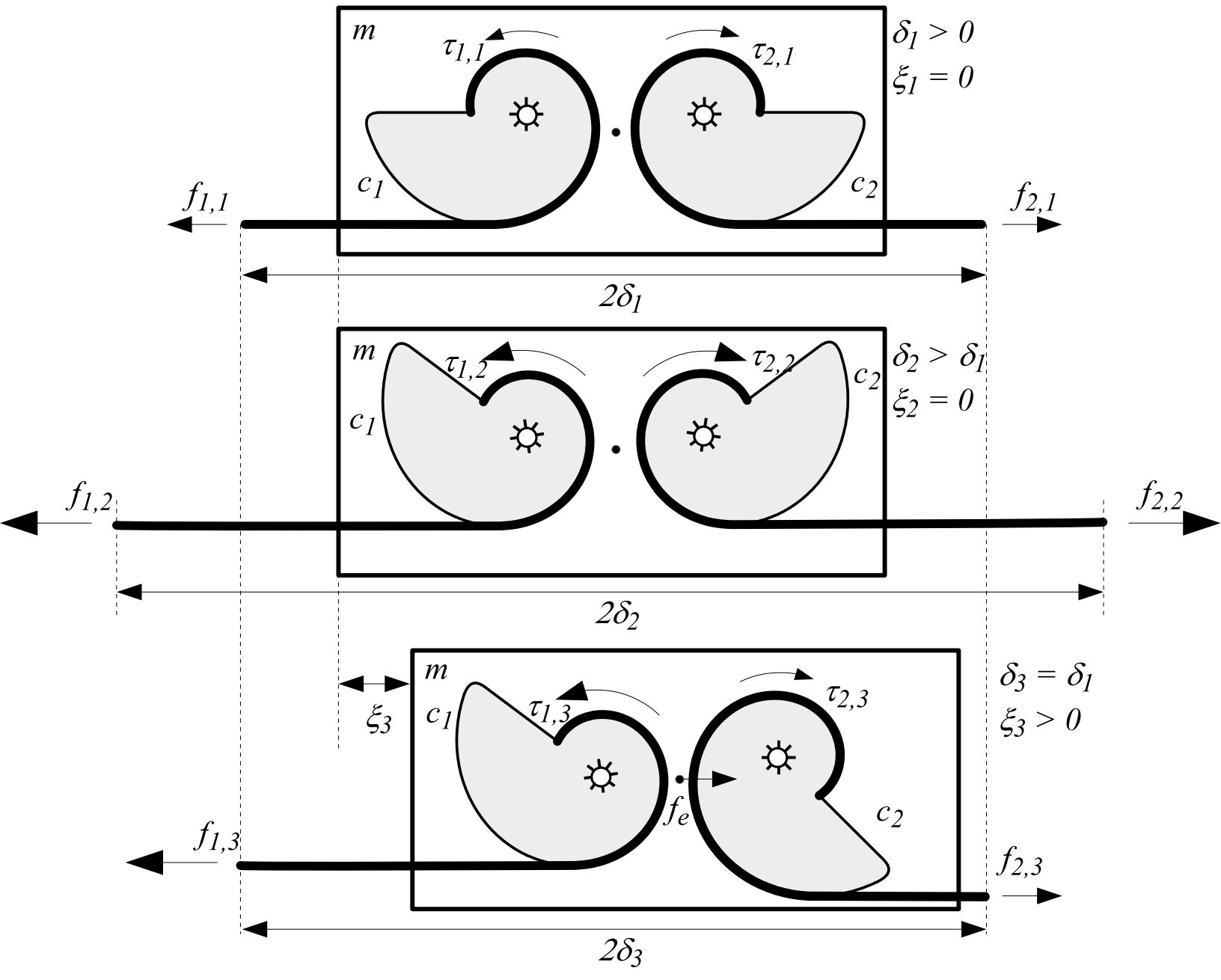

poly_opt_linwwcvsa_cam.eps

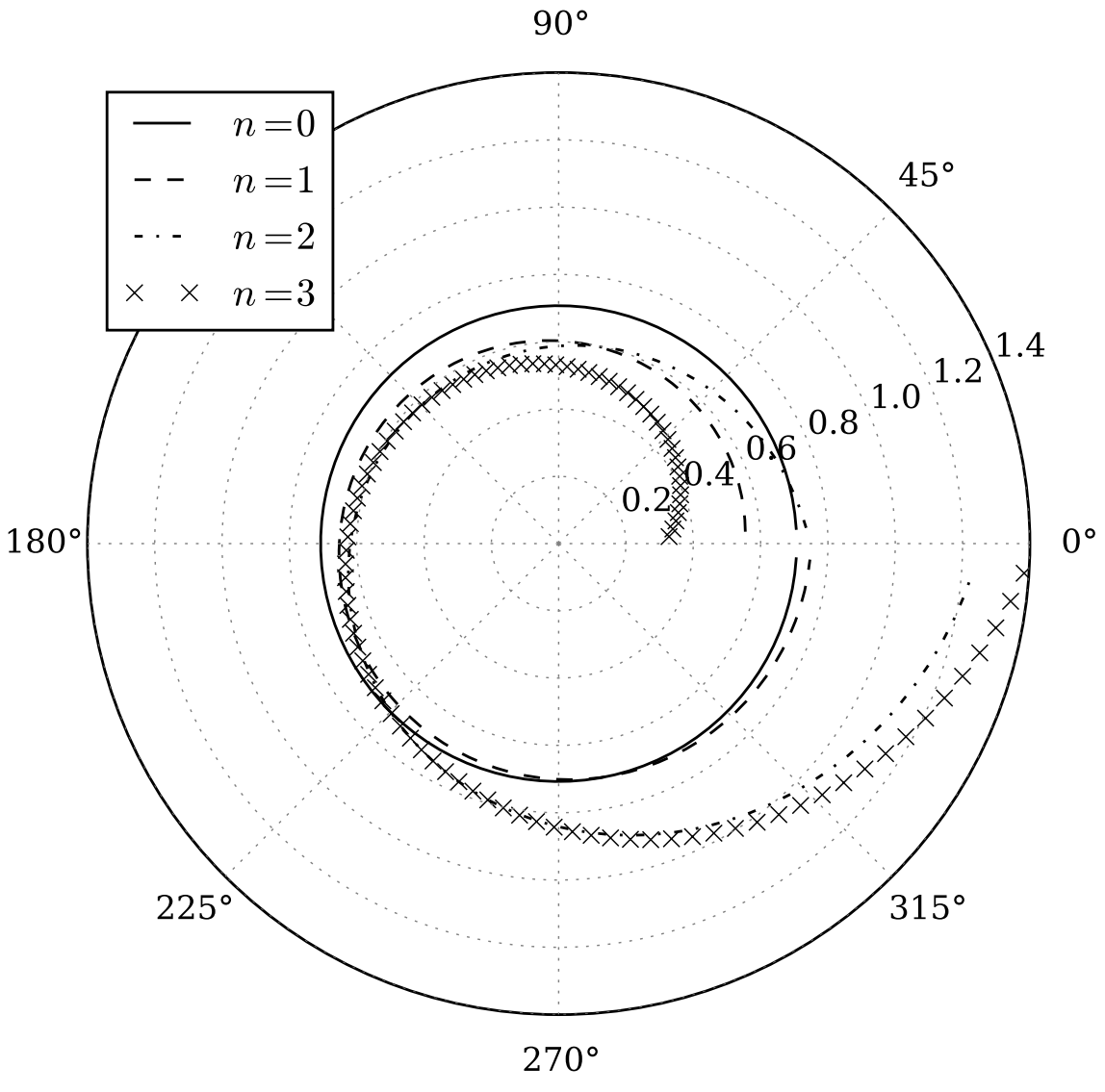

poly_opt_linwwcvsa_x_kl.eps

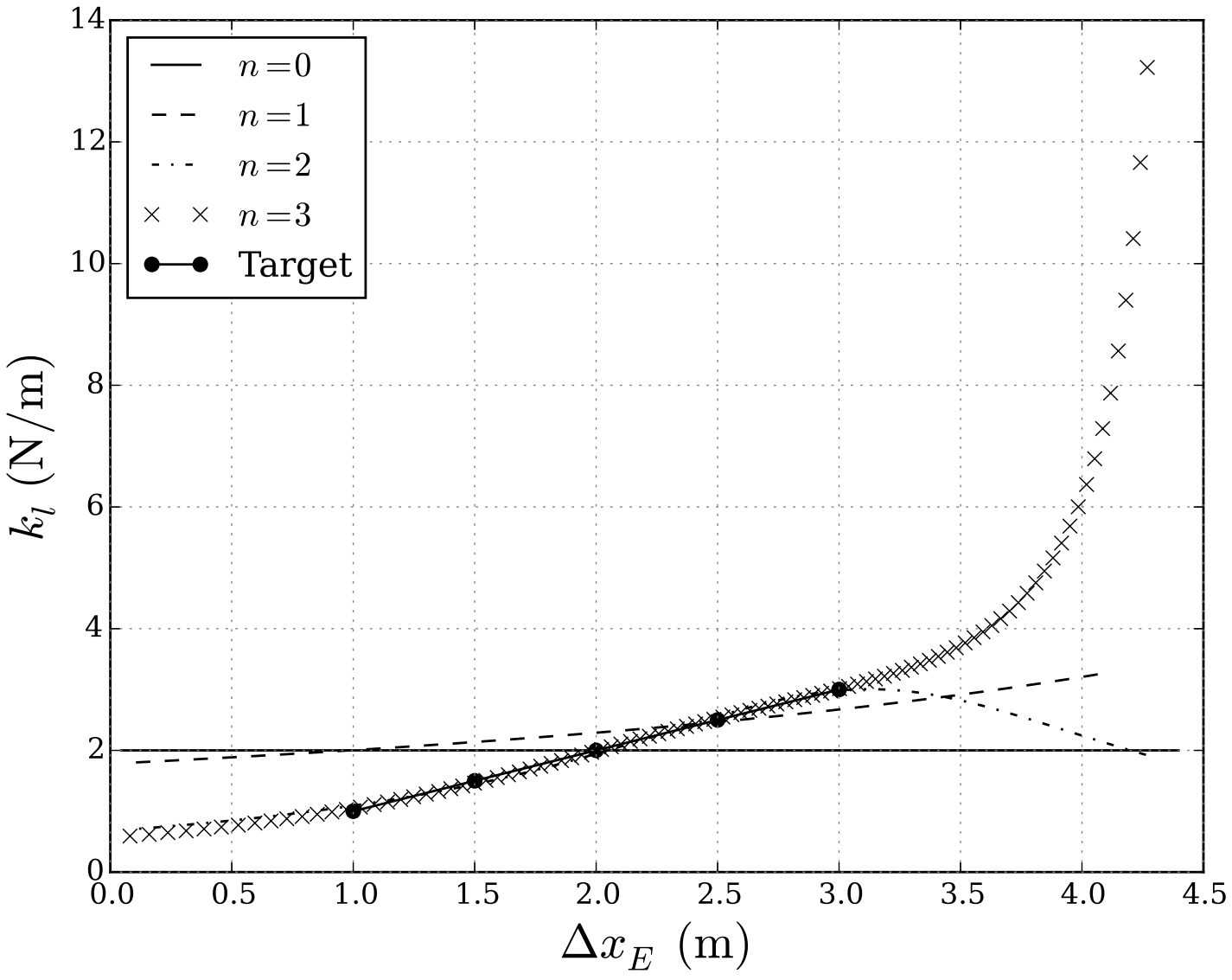

poly_opt_linwwcvsa_x_kl_zoom.eps

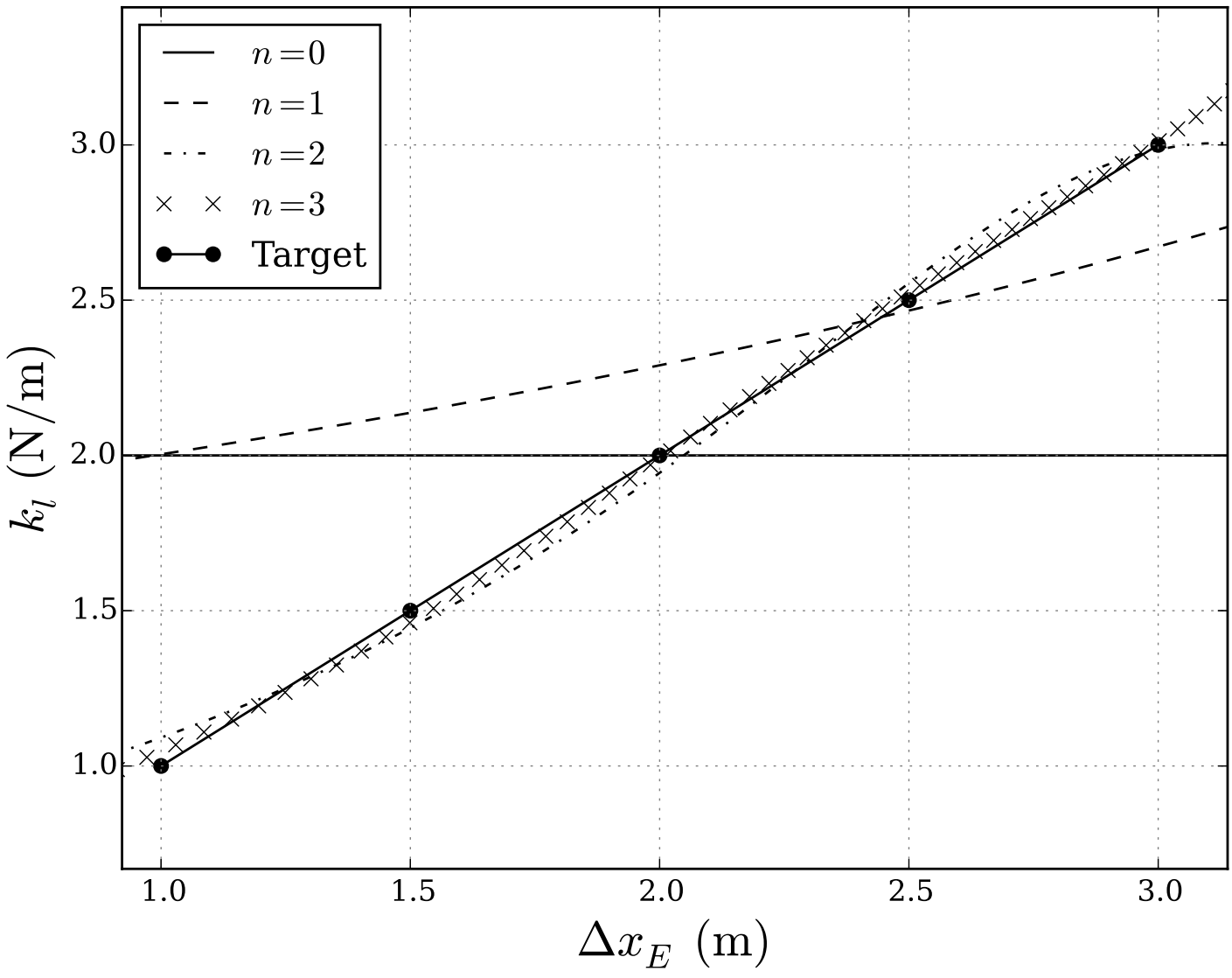

**norm_linwwcvsa_with_pulley_5rad.eps**

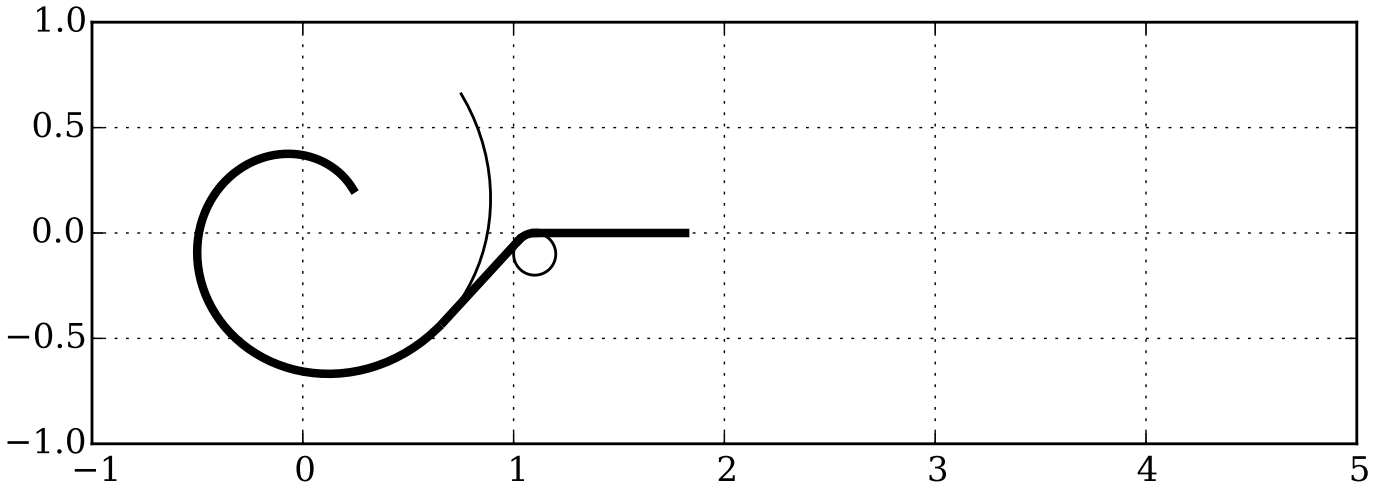

**norm_linwwcvsa_with_pulley_4rad.eps**

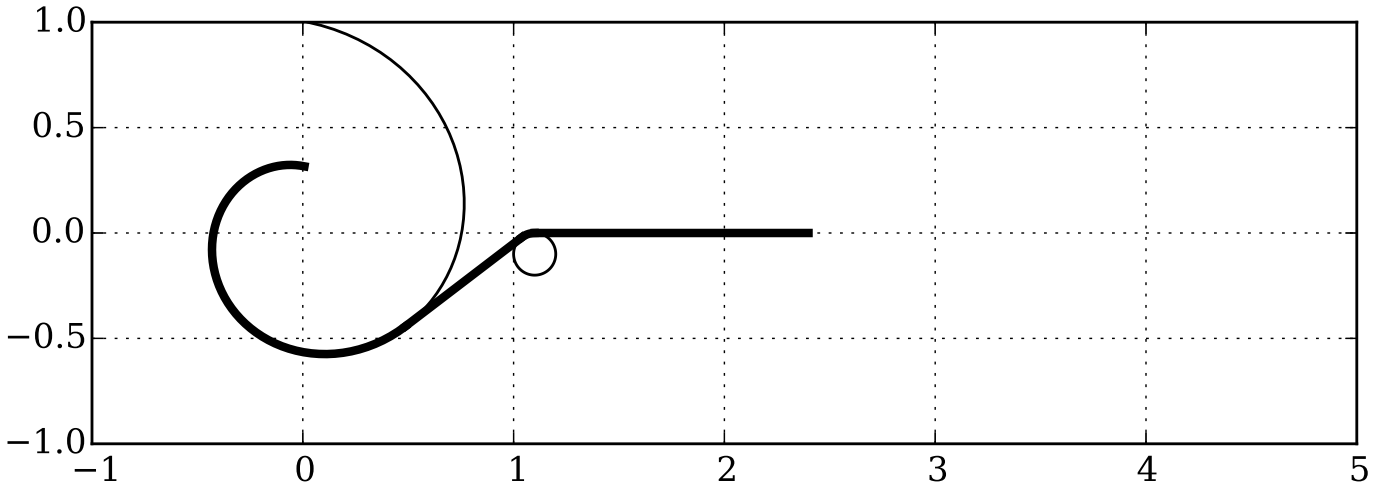

**norm_linwwcvsa_with_pulley_3rad.eps**

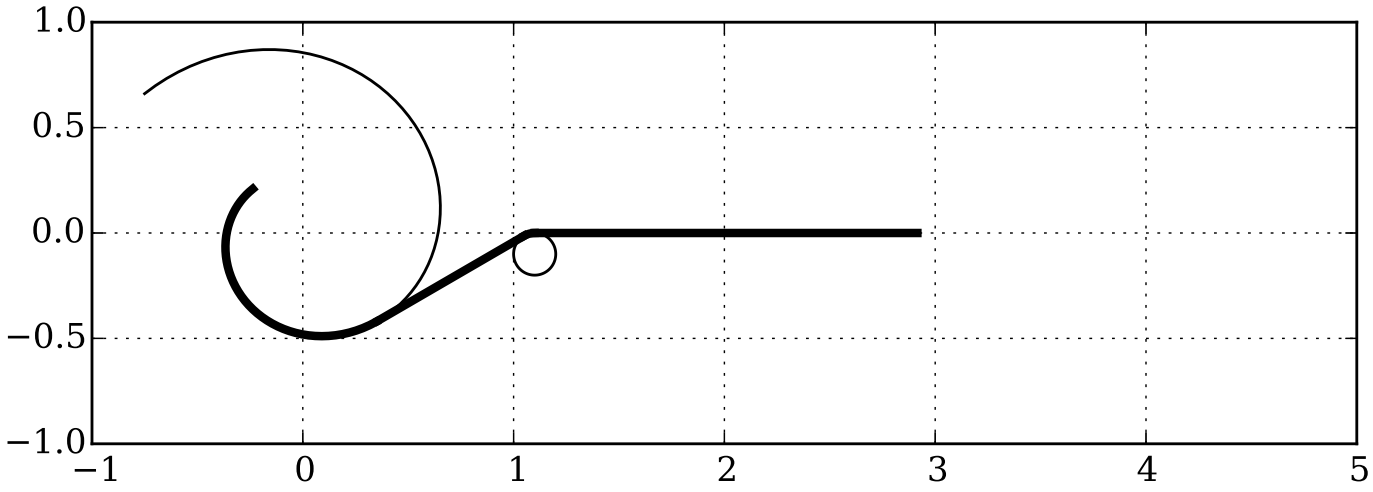

**norm_linwwcvsa_with_pulley_2rad.eps**

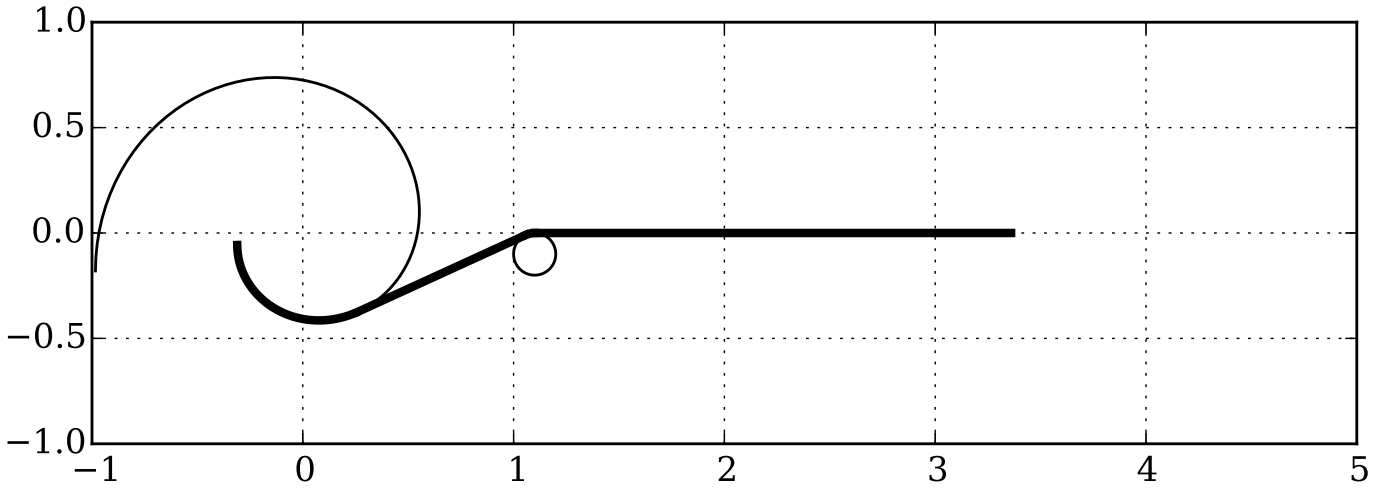

**norm_linwwcvsa_with_pulley_1rad.eps**

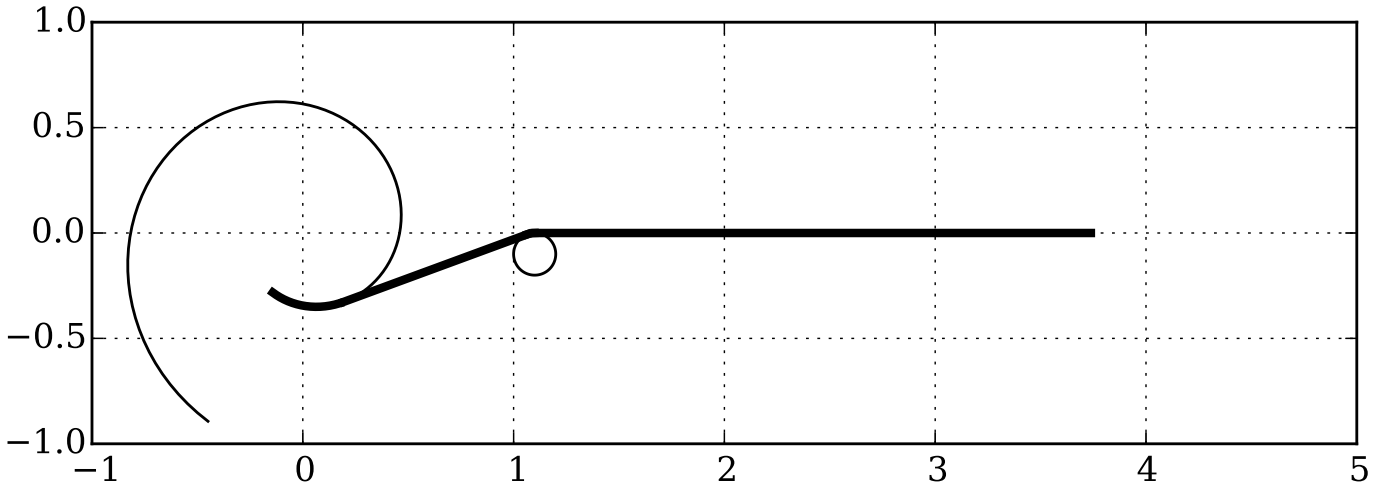

**norm_linwwcvsa_with_pulley_0rad.eps**

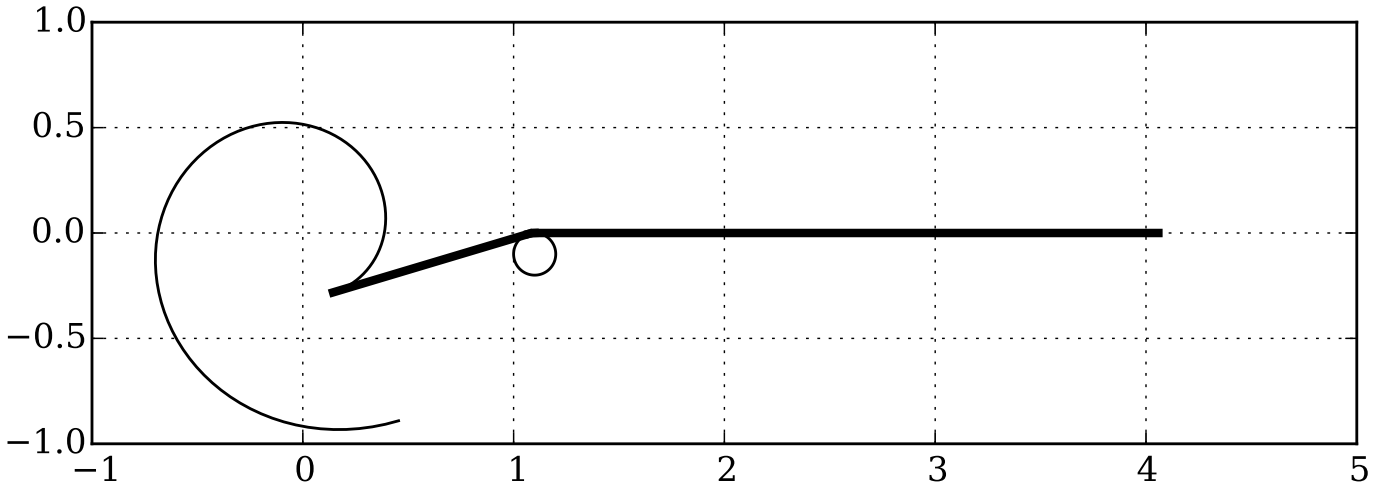

**norm_linwwcvsa_with_wo_pulley_x_gamma.eps**

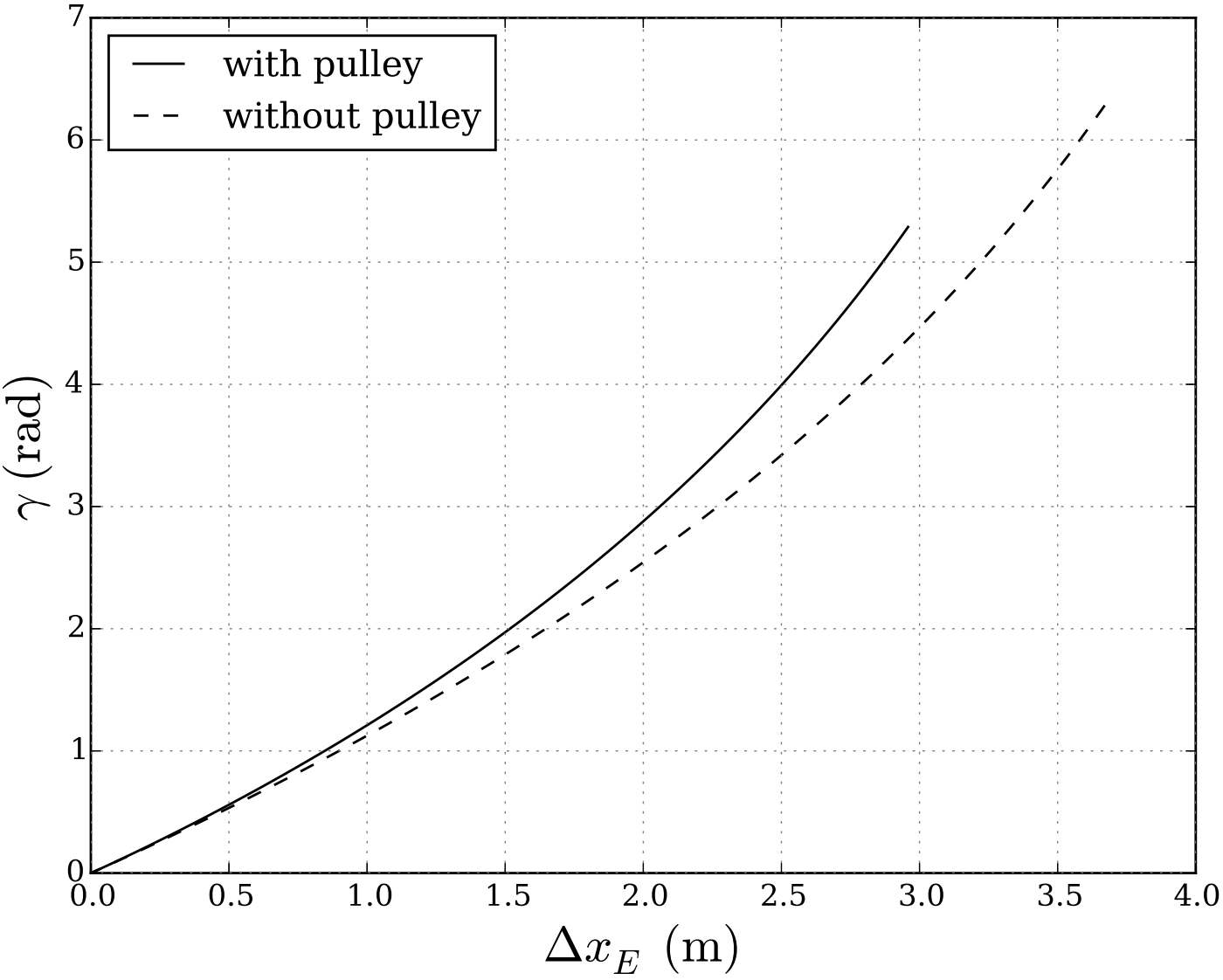

**norm_linwwcvsa_with_wo_pulley_x_kt.eps**

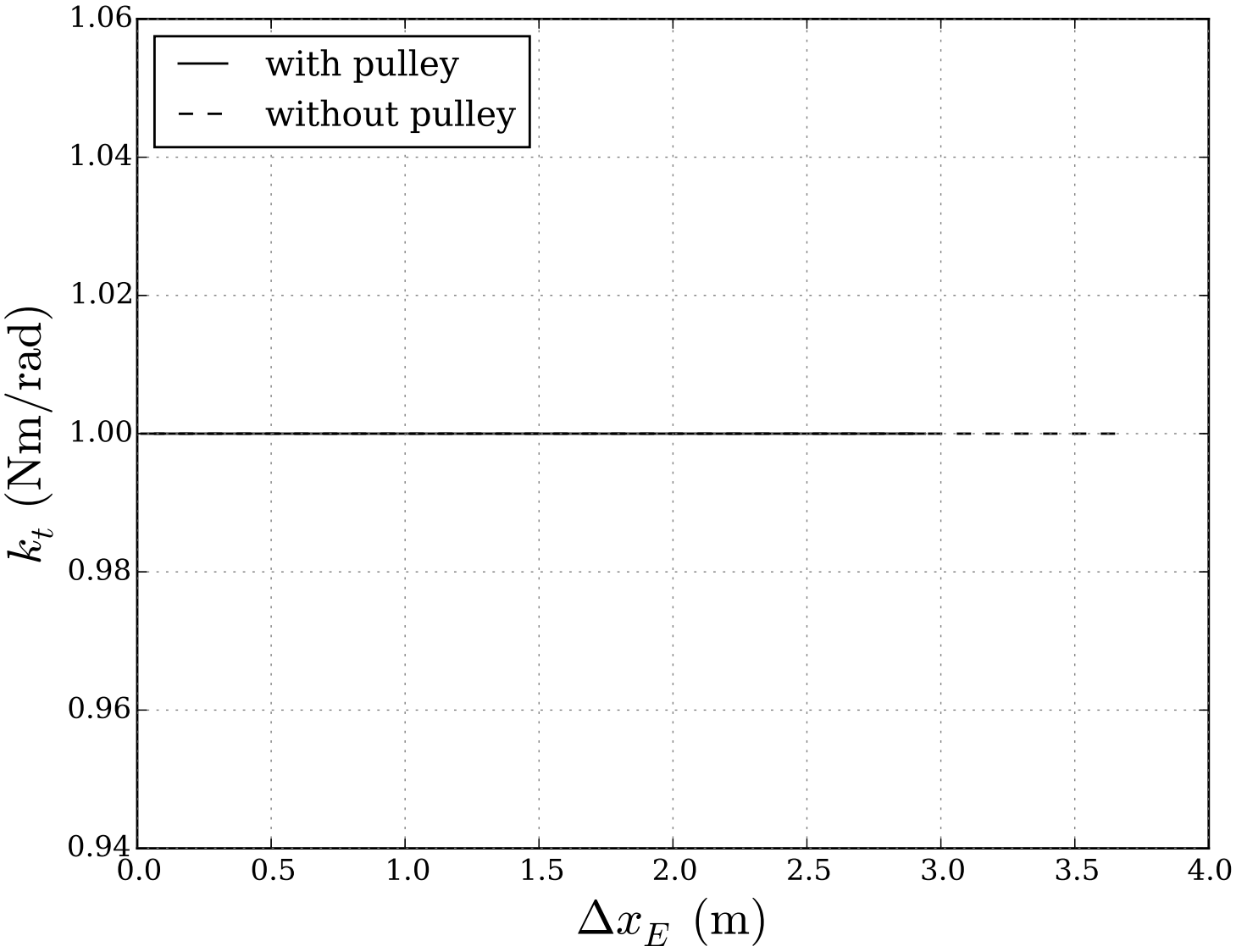

**norm_linwwcvsa_with_wo_pulley_x_kl.eps**

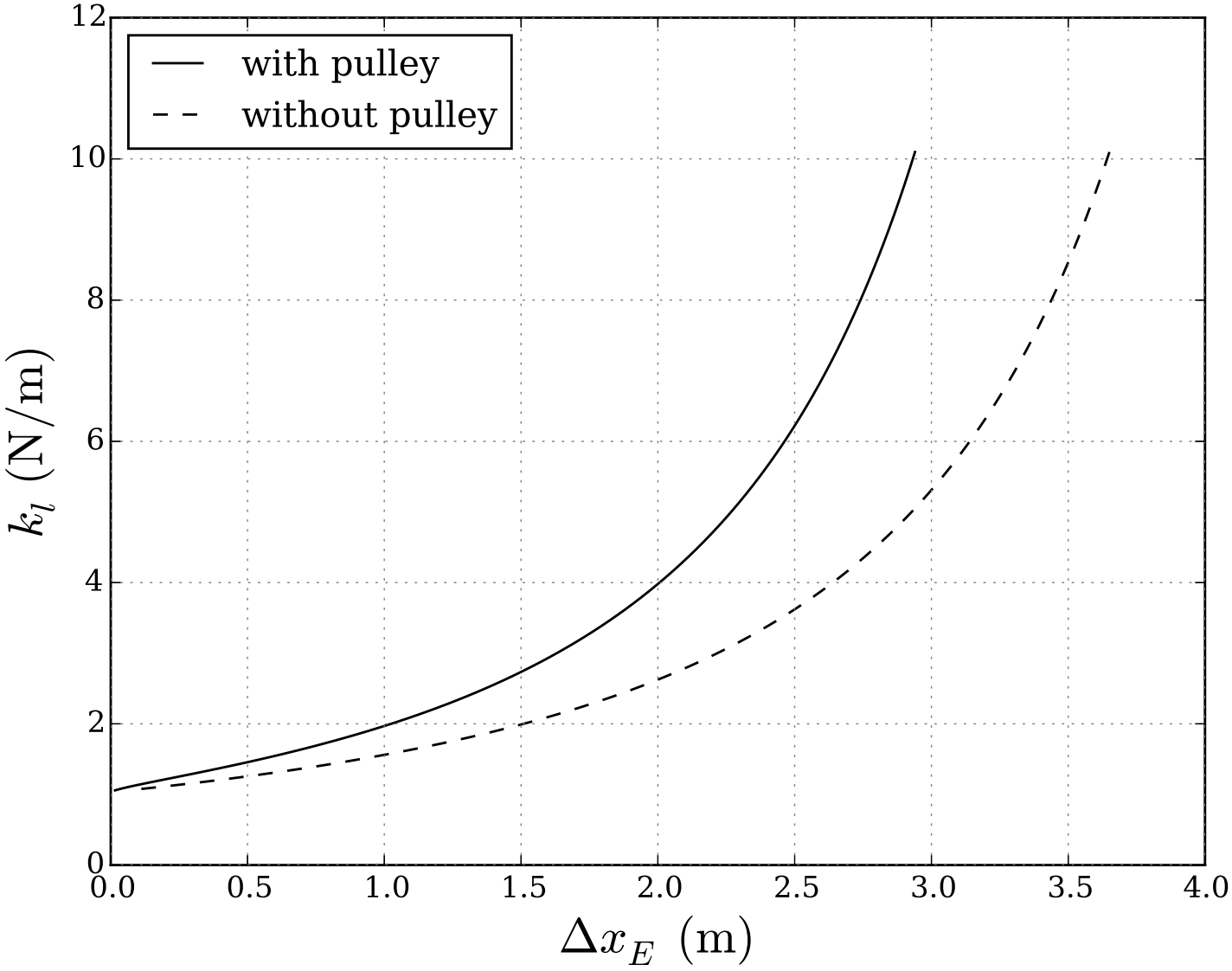

**norm_linwwcvsa_with_wo_pulley_x_tau.eps**

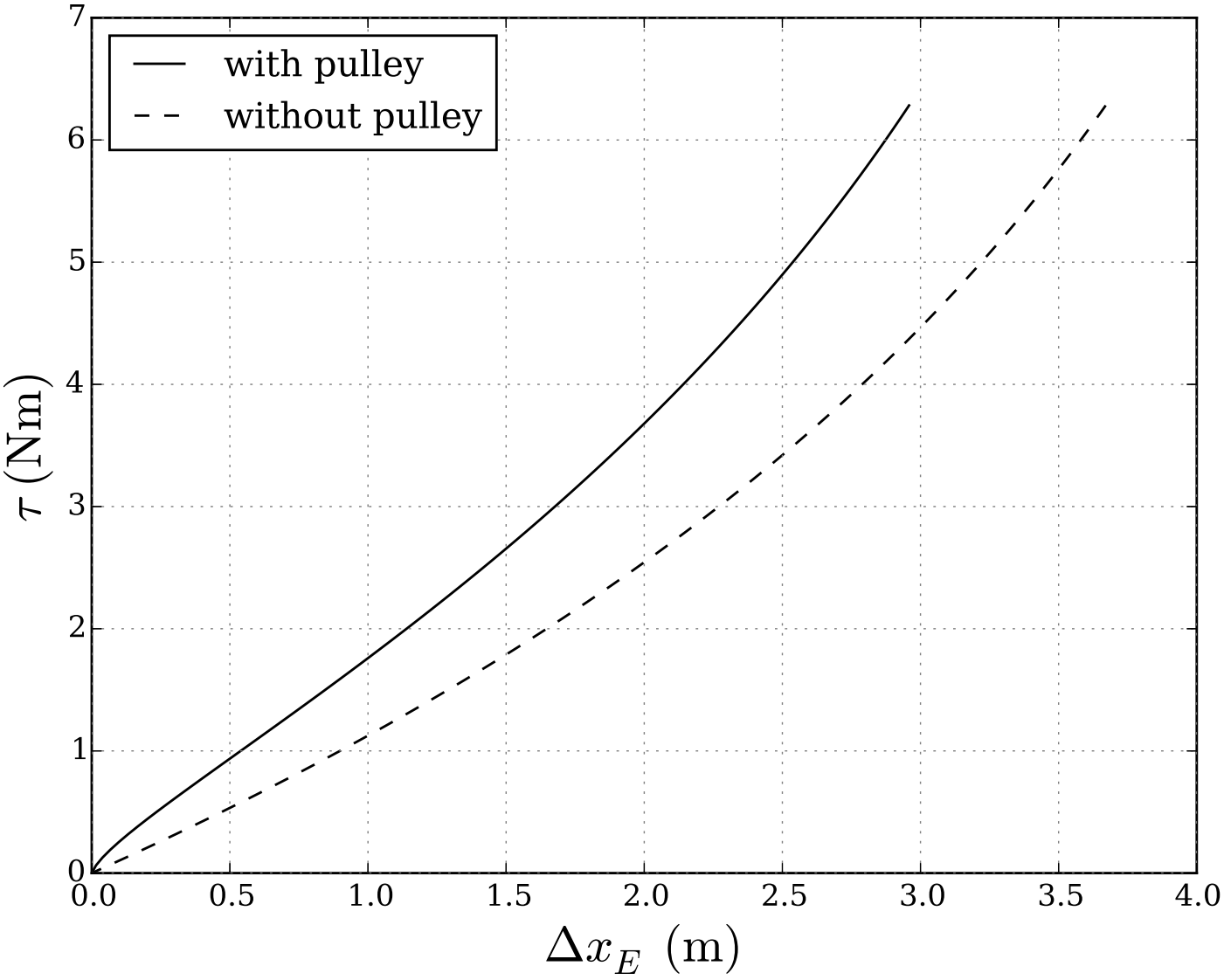

**norm_linwwcvsa_with_wo_pulley_x_f.eps**

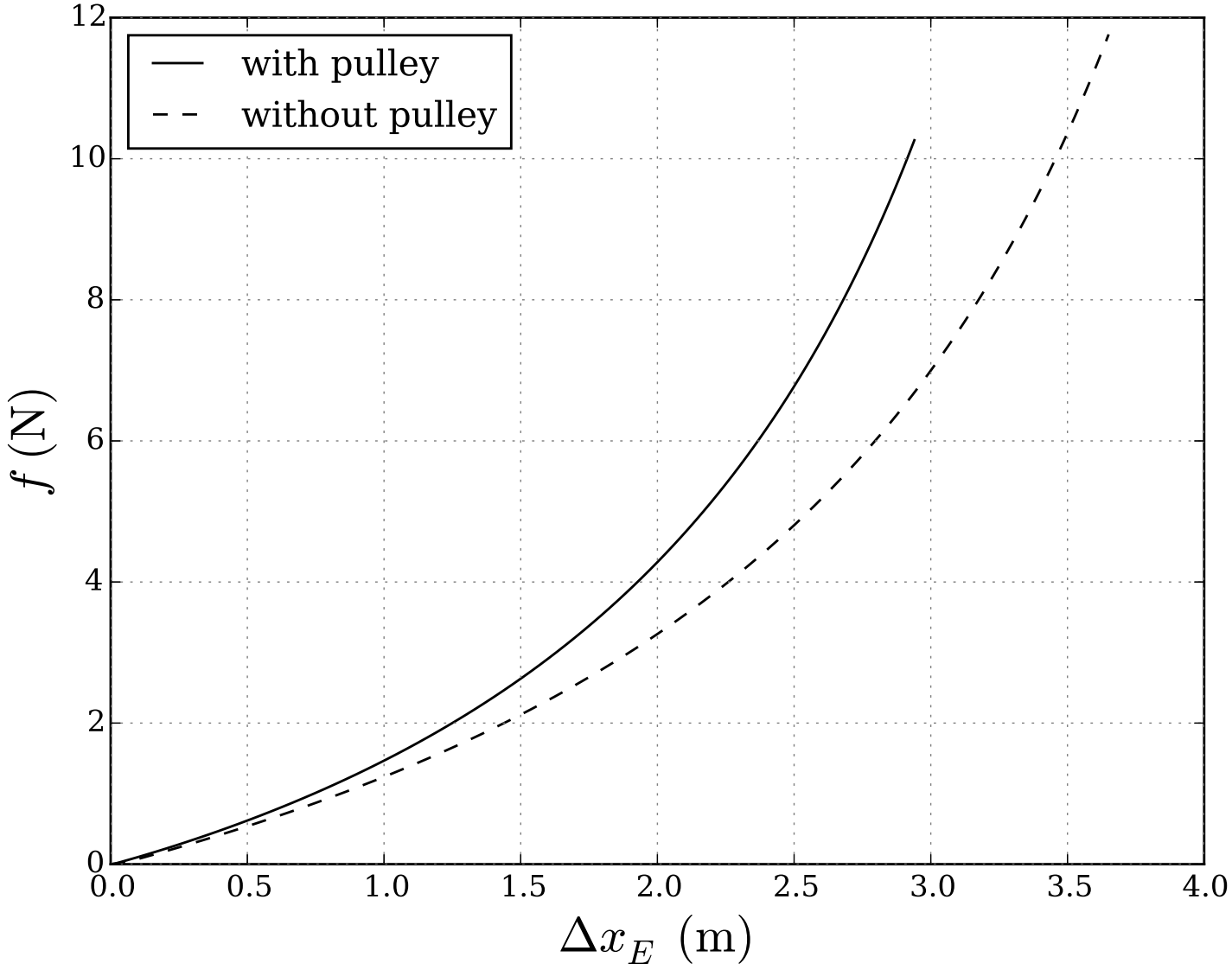

delta_xi_force_norm_linwwcvsa_with_pulley.eps

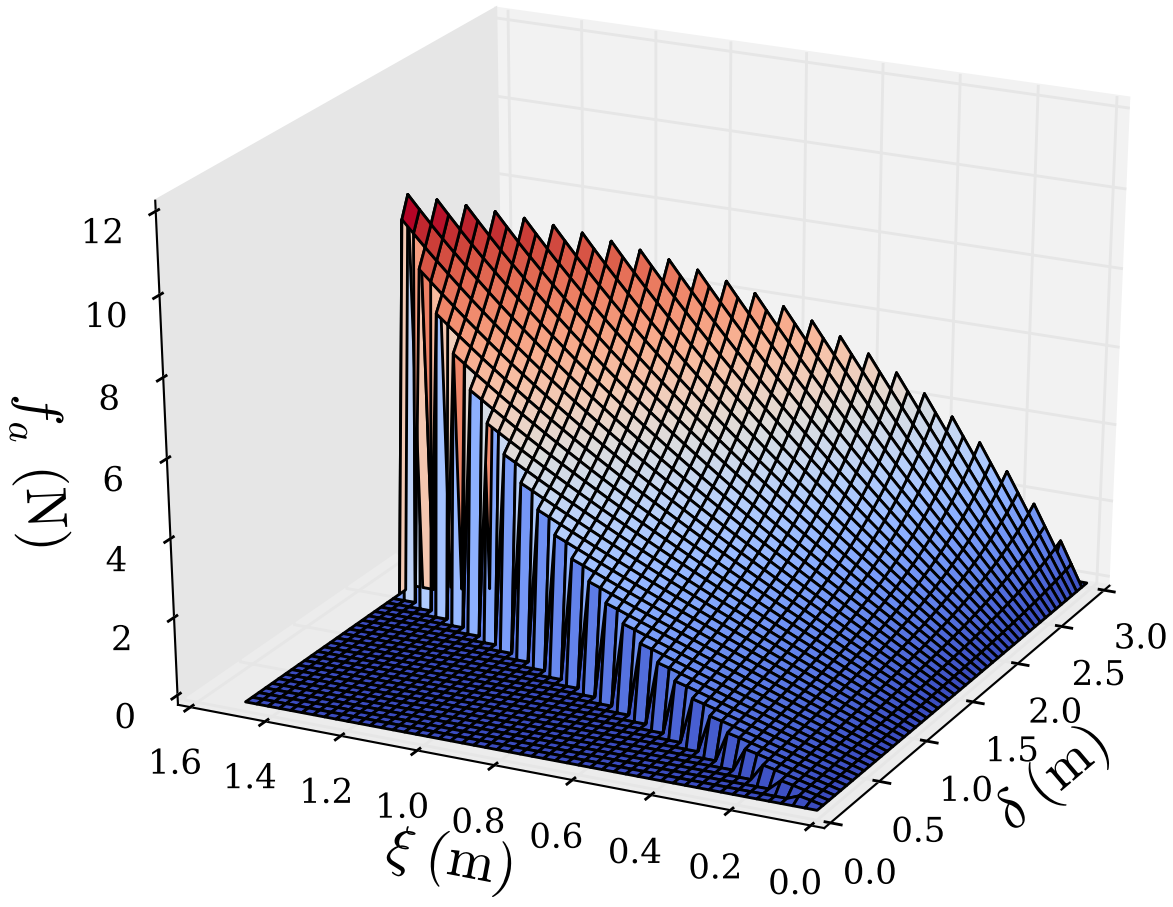

delta_xi_stiffness_norm_linwwcvsa_with_pulley.eps

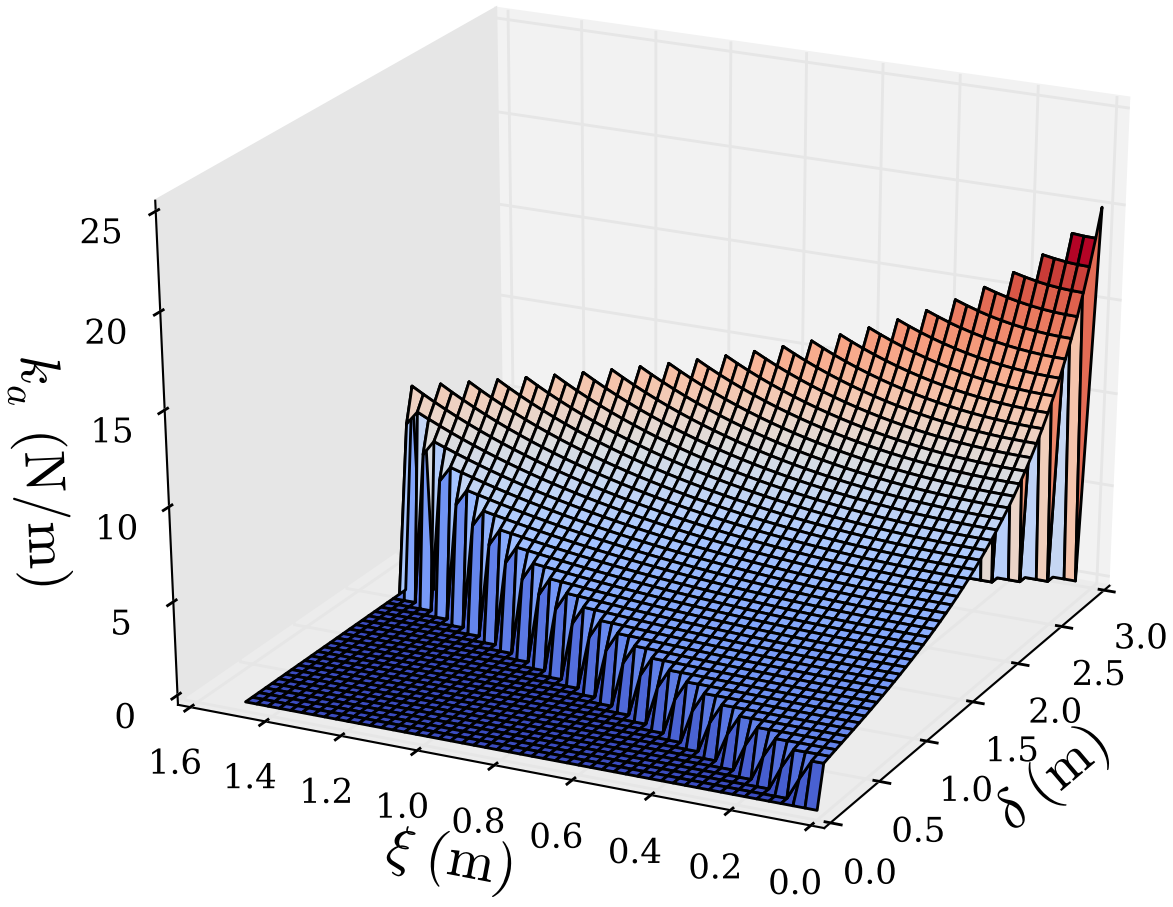

cam_with_pulley.eps

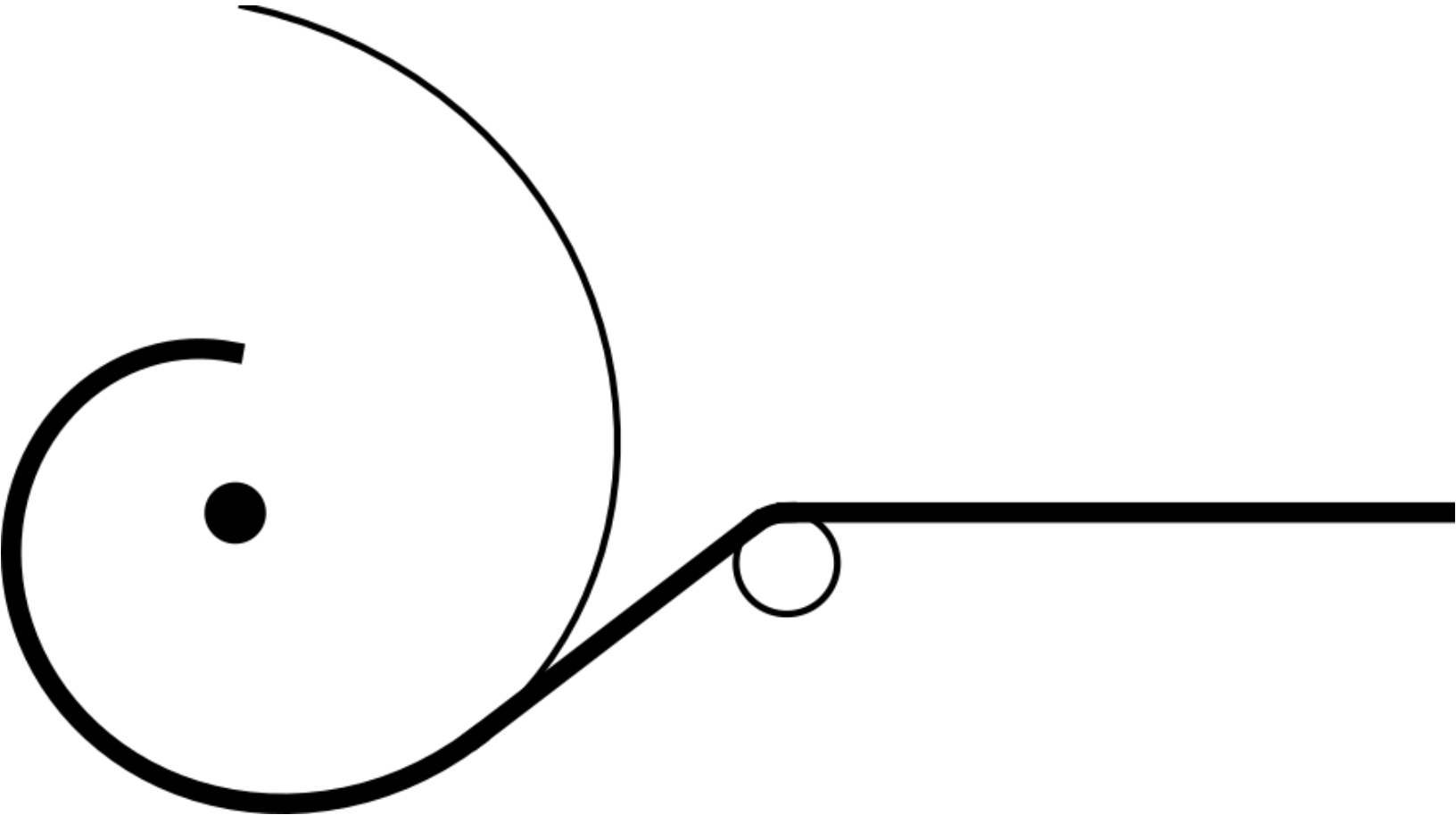

cam_without_pulley.eps

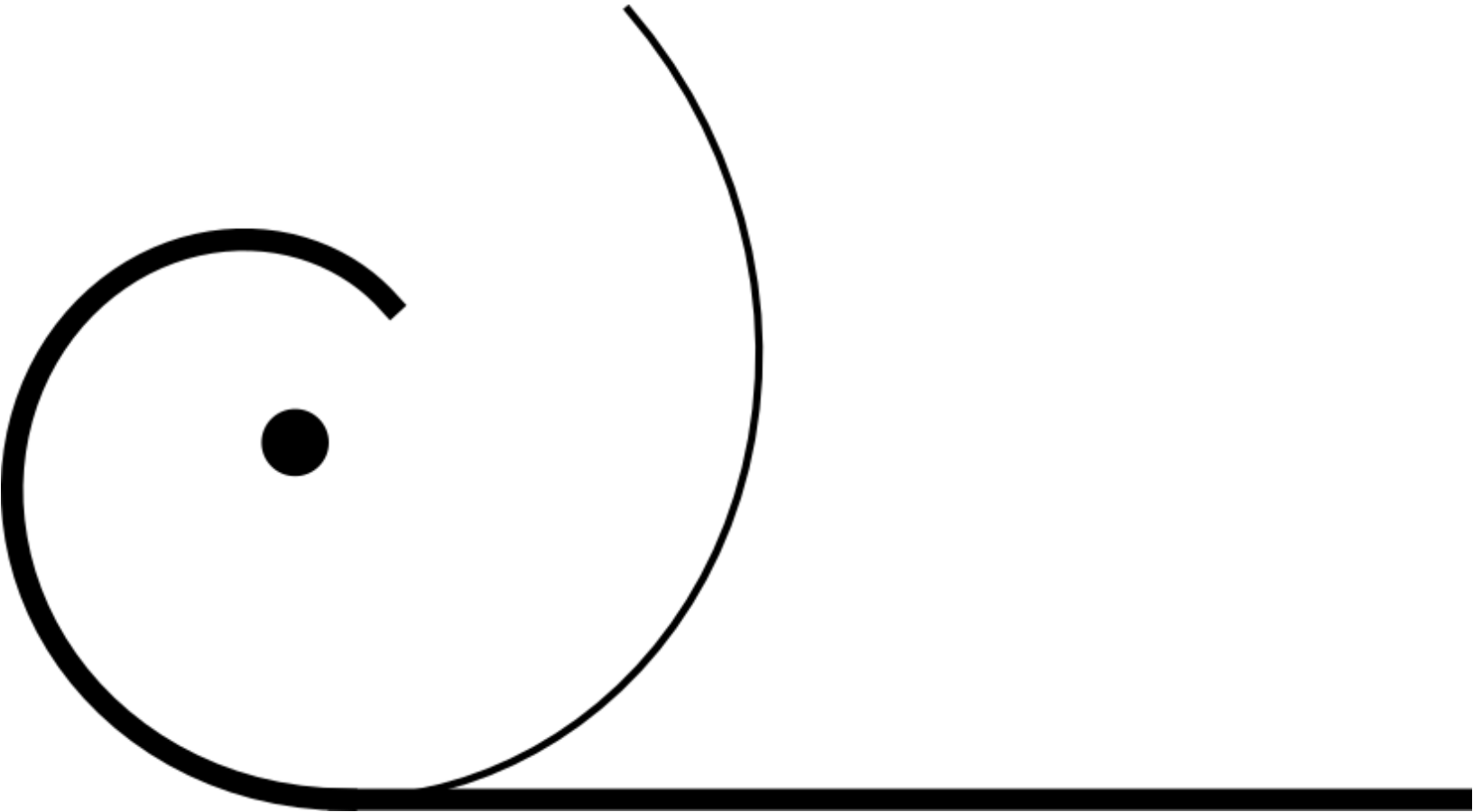

cam_vsa_coplanar.eps

cam_vsa_coaxial.eps

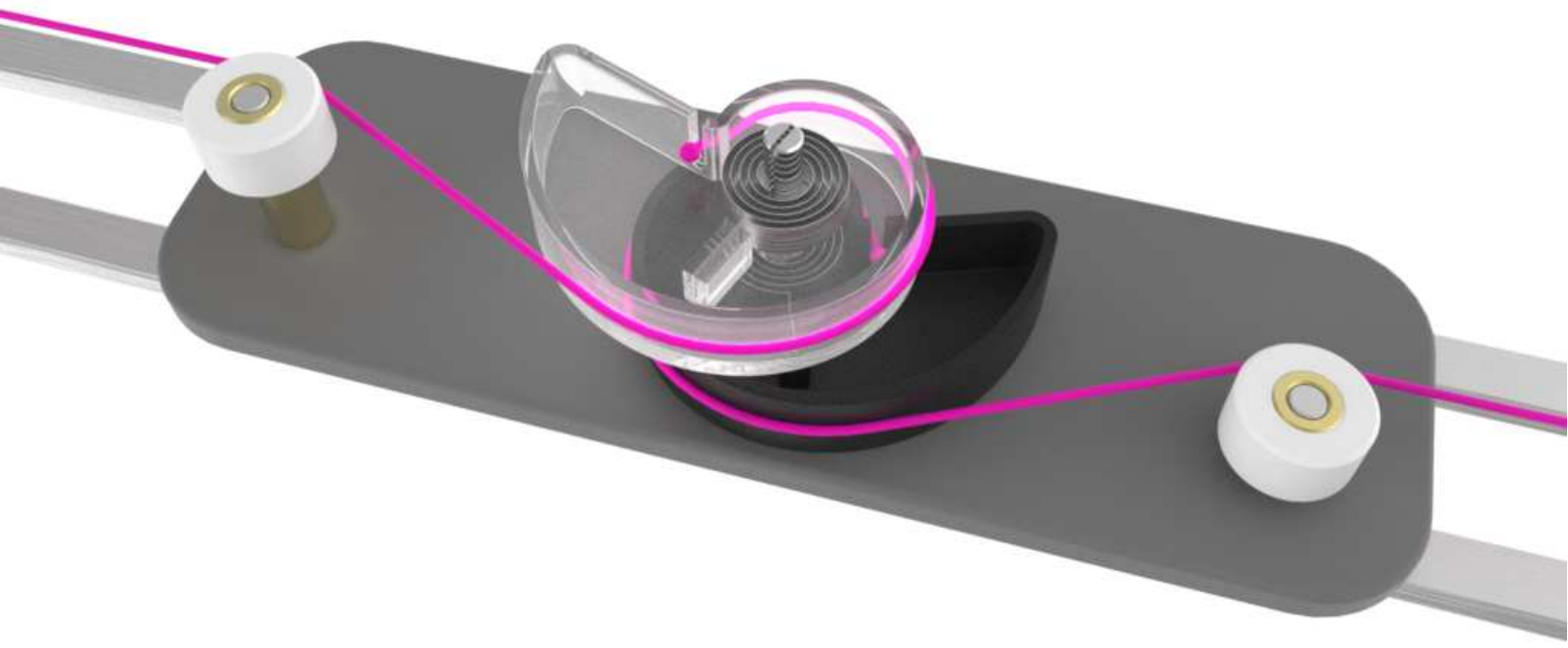

**linarm2_assembly.eps**

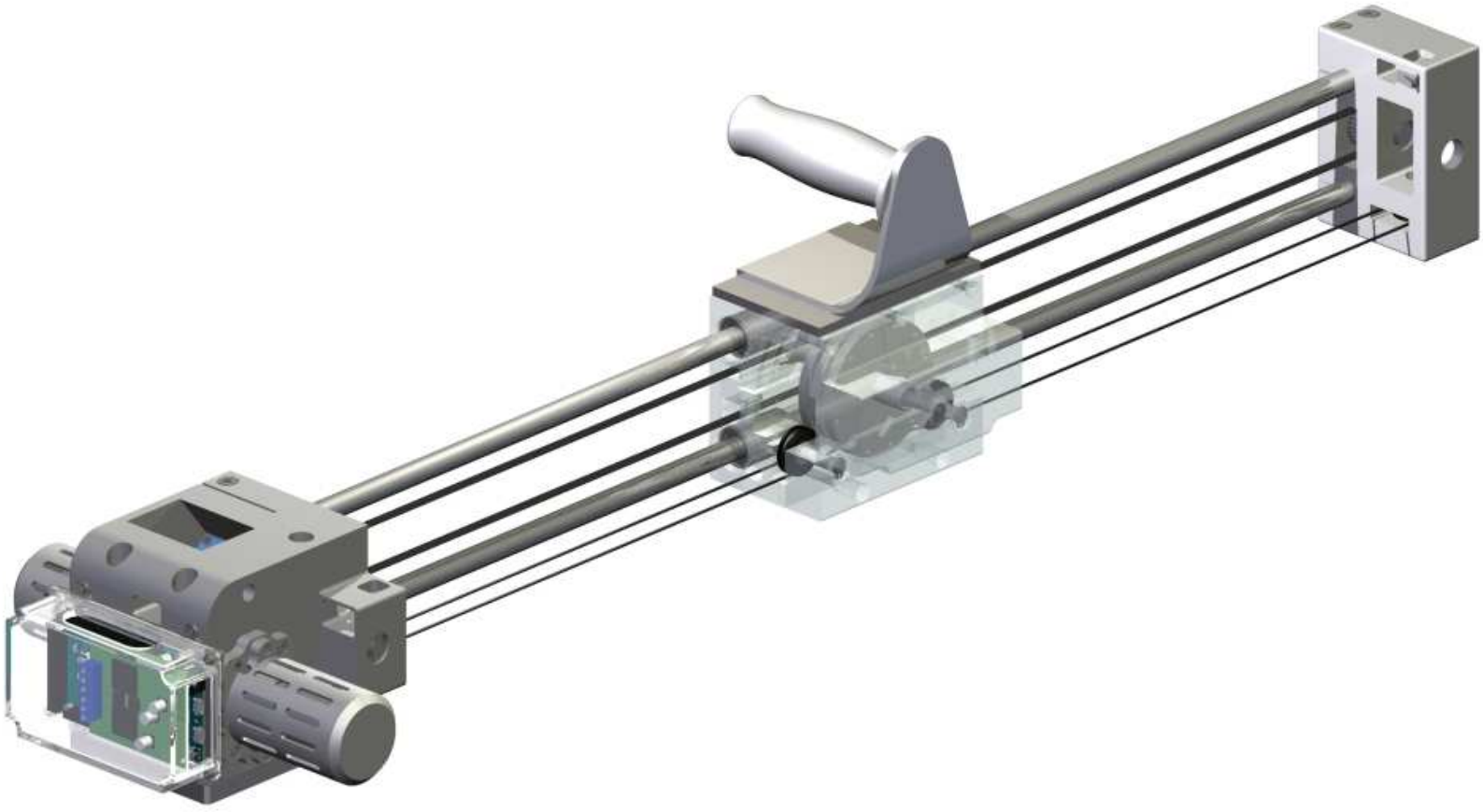

multiple_turns_cam.eps

**planar_vsa.eps**

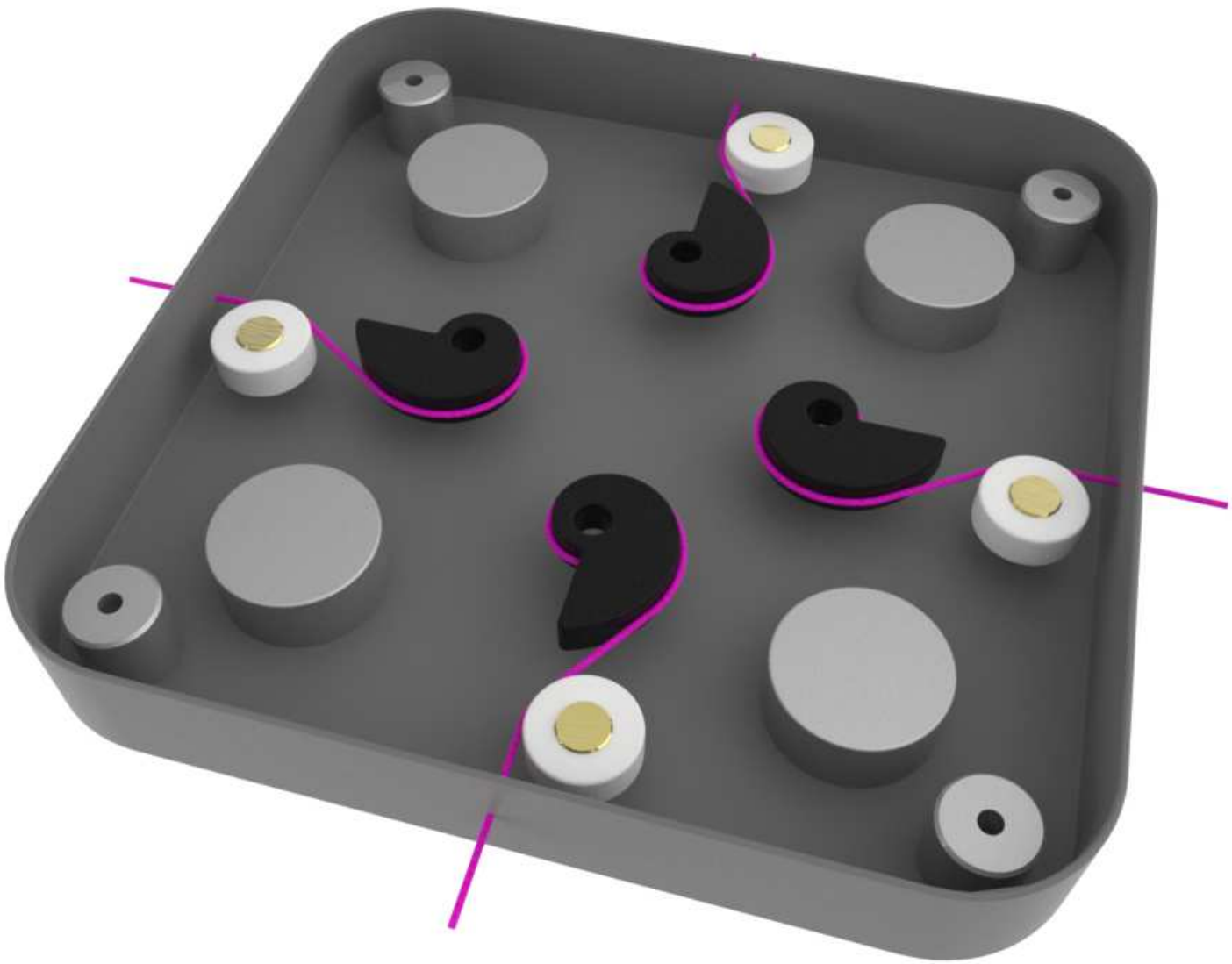

**vsa_cam_mmt.tex**

**Click here to download LaTeX Source Files: vsa_cam_mmt.tex**

**Bibliography (.bib format)**

**Click here to download LaTeX Source Files: phd_mm.bib**